

Tidal evolution of exoplanets

Alexandre C.M. Correia

University of Aveiro

Jacques Laskar

Paris Observatory

Tidal effects arise from differential and inelastic deformation of a planet by a perturbing body. The continuous action of tides modify the rotation of the planet together with its orbit until an equilibrium situation is reached. It is often believed that synchronous motion is the most probable outcome of the tidal evolution process, since synchronous rotation is observed for the majority of the satellites in the Solar System. However, in the XIXth century, Schiaparelli also assumed synchronous motion for the rotations of Mercury and Venus, and was later shown to be wrong. Rather, for planets in eccentric orbits synchronous rotation is very unlikely. The rotation period and axial tilt of exoplanets is still unknown, but a large number of planets have been detected close to the parent star and should have evolved to a final equilibrium situation. Therefore, based on the Solar System well studied cases, we can make some predictions for exoplanets. Here we describe in detail the main tidal effects that modify the secular evolution of the spin and the orbit of a planet. We then apply our knowledge acquired from Solar System situations to exoplanet cases. In particular, we will focus on two classes of planets, “Hot-Jupiters” (fluid) and “Super-Earths” (rocky with atmosphere).

1. INTRODUCTION

The occurrence, on most open ocean coasts, of high sea tide at about the time of Moon’s passage across the meridian, early prompted the idea that Earth’s satellite exerts an attraction on the water. The occurrence of a second high tide when the Moon is on the opposite meridian was a great puzzle, but the correct explanation of the tidal phenomena was given by Newton in “*Philosophiæ Naturalis Principia Mathematica*”. Tides are a consequence of the lunar and solar gravitational forces acting in accordance with laws of mechanics. Newton realized that the tidal forces also must affect the atmosphere, but he assumed that the atmospheric tides would be too small to be detected, because changes in weather would introduce large irregular variations upon barometric measurements.

However, the semi-diurnal oscillations of the atmospheric surface pressure has proven to be one of the most regular of all meteorological phenomena. It is readily detectable by harmonic analysis at any station over the world (e.g. Chapman and Lindzen 1970). The main difference in respect to ocean tides is that atmospheric tides follow the Sun and not the Moon, as the atmosphere is essentially excited by the Solar heat. Even though tides of gravitational origin are present in the atmosphere, the thermal tides are more important as the pressure variations on the ground are more sensitive to the temperature gradients than to the gravitational ones.

The inner planets of the Solar System as well as the majority of the main satellites present today a spin different from what is believed to have been the initial one

(e.g. Goldreich and Soter 1966; Goldreich and Peale 1968). Planets and satellites are supposed to rotate much faster in the beginning and any orientation of the spin axis may be allowed (e.g. Dones and Tremaine 1993; Kokubo and Ida 2007). However, tidal dissipation within the internal layers give rise to secular evolution of planetary spins and orbits. In the case of the satellites, spin and orbital evolution is mainly driven by tidal interactions with the central planet, whereas for the inner planets the main source of tidal dissipation is the Sun (in the case of the Earth, tides raised by the Moon are also important).

Orbital and spin evolution cannot be dissociated because the total angular momentum must be conserved. As a consequence a reduction in the rotation rate of a body implies an increment of the orbit semi-major axis and vice-versa. For instance, the Earth’s rotation period is increasing about 2 ms/century (e.g. Williams 1990), and the Moon is consequently moving away about 3.8 cm/year (e.g. Dickey et al. 1994). On the other hand, Neptune’s moon, Triton, and the Martian moon, Phobos, are spiraling down into the planet, clearly indicating that the present orbits are not primordial, and may have undergone a long evolving process from a previous capture from an heliocentric orbit (e.g. Mignard 1981; Goldreich et al. 1989; Correia 2009). Both the Earth’s Moon and Pluto’s moon, Charon, have a significant fraction of the mass of their systems, and therefore they could be classified as double-planets rather than as satellites. The proto-planetary disk is unlikely to produce double-planet systems, whose origin seems to be due to a catastrophic impact of the initial planet with a body of comparable dimensions (e.g. Canup and Asphaug 2001;

mentum on the C axis, with rotation rate $\omega = \dot{\theta} - \dot{\psi} \cos \varepsilon$, and $X = \mathbf{L} \cdot \mathbf{k}$ is the projection of the angular momentum on the normal to the ecliptic; θ is the hour angle between the equinox of date and a fixed point of the equator, and ψ is the general precession angle, an angle that simultaneously accounts for the precession of the spin axis and the orbit (Fig. 1).

2.1.1. Gravitational potential

The gravitational potential V (energy per unit mass) generated by the planet at a generic point of the space \mathbf{r} , expanded in degree two of R/r , where R is the planet's radius, is given by (e.g. Tisserand 1891; Smart 1953):

$$V(\mathbf{r}) = -\frac{Gm}{r} + \frac{G(B-A)}{r^3} P_2(\hat{\mathbf{r}} \cdot \mathbf{J}) + \frac{G(C-A)}{r^3} P_2(\hat{\mathbf{r}} \cdot \mathbf{K}), \quad (1)$$

where $\hat{\mathbf{r}} = \mathbf{r}/r$, G is the gravitational constant, and $P_2(x) = (3x^2 - 1)/2$ are the Legendre polynomials of degree two. The potential energy U when orbiting a central star of mass m_* is then:

$$U = m_* V(\mathbf{r}). \quad (2)$$

For a planet evolving in a non-perturbed keplerian orbit, we write:

$$\hat{\mathbf{r}} = \cos(\varpi + v)\mathbf{i} + \sin(\varpi + v)\mathbf{j}, \quad (3)$$

where ϖ is the longitude of the periape and v the true anomaly (see Chapter 2: *Keplerian Orbits and Dynamics*). Thus, transforming the body equatorial frame ($\mathbf{I}, \mathbf{J}, \mathbf{K}$) into the orbital frame ($\mathbf{i}, \mathbf{j}, \mathbf{k}$), we obtain (Fig. 1):

$$\begin{cases} \hat{\mathbf{r}} \cdot \mathbf{J} = -\cos w \sin \theta + \sin w \cos \theta \cos \varepsilon, \\ \hat{\mathbf{r}} \cdot \mathbf{K} = -\sin w \sin \varepsilon, \end{cases} \quad (4)$$

where $w = \varpi + \psi + v$ is the true longitude of date. The expression for the potential energy (Eq. 2) becomes (e.g. Correia 2006):

$$U = -\frac{Gmm_*}{r} + \frac{GCm_*}{r^3} E_d P_2(\sin w \sin \varepsilon) - \frac{3Gm_*}{8r^3} (B-A) F(\theta, w, \varepsilon), \quad (5)$$

where

$$F(\theta, w, \varepsilon) = 2 \cos(2\theta - 2w) \cos^4 \left(\frac{\varepsilon}{2} \right) + 2 \cos(2\theta + 2w) \sin^4 \left(\frac{\varepsilon}{2} \right) + \cos(2\theta) \sin^2 \varepsilon, \quad (6)$$

and

$$E_d = \frac{C - \frac{1}{2}(A+B)}{C} = \frac{k_f R^5}{3GC} \omega^2 + \delta E_d, \quad (7)$$

where E_d is the dynamical ellipticity, and k_f is the fluid Love number (pertaining to a perfectly fluid body with the same mass distribution as the actual planet). The first part of E_d (Eq. 7) corresponds to the flattening in hydrostatic equilibrium (Lambeck 1980), and δE_d to the departure from this equilibrium.

2.1.2. Averaged potential

Since we are only interested in the study of the long-term motion, we will average the potential energy U over the rotation angle θ and the mean anomaly M :

$$\bar{U} = \frac{1}{4\pi^2} \int_0^{2\pi} \int_0^{2\pi} U dM d\theta. \quad (8)$$

However, when the rotation frequency $\omega \approx \dot{\theta}$ and the mean motion $n = \dot{M}$ are close to resonance ($\omega \approx pn$, for a semi-integer value p), the terms with argument $2(\theta - pM)$ vary slowly and must be retained in the expansions (e.g. Murray and Dermott 1999)

$$\frac{\cos(2\theta)}{r^3} = \frac{1}{a^3} \sum_{p=-\infty}^{+\infty} G(p, e) \cos 2(\theta - pM), \quad (9)$$

and

$$\frac{\cos(2\theta - 2w)}{r^3} = \frac{1}{a^3} \sum_{p=-\infty}^{+\infty} H(p, e) \cos 2(\theta - pM), \quad (10)$$

where a and e are the semi-major axis and the eccentricity of the planet's orbit, respectively. The functions $G(p, e)$ and $H(p, e)$ can be expressed in power series in e (Table 1). The averaged non-constant part of the potential \bar{U} becomes:

$$\begin{aligned} \frac{\bar{U}}{C} = & -\alpha \frac{\omega x^2}{2} - \frac{\beta}{4} \left[(1-x^2) G(p, e) \cos 2(\theta - pM) \right. \\ & + \frac{(1+x)^2}{2} H(p, e) \cos 2(\theta - pM - \phi) \\ & \left. + \frac{(1-x)^2}{2} H(-p, e) \cos 2(\theta - pM + \phi) \right], \end{aligned} \quad (11)$$

where $x = X/L = \cos \varepsilon$, $\phi = \varpi + \psi$,

$$\alpha = \frac{3Gm_*}{2a^3(1-e^2)^{3/2}} \frac{E_d}{\omega} \approx \frac{3n^2}{2\omega} (1-e^2)^{-3/2} E_d \quad (12)$$

is the ‘‘precession constant’’ and

$$\beta = \frac{3Gm_*}{2a^3} \frac{B-A}{C} \approx \frac{3}{2} n^2 \frac{B-A}{C}. \quad (13)$$

For non-resonant motion, that is, when $(B-A)/C \approx 0$ (e.g. gaseous planets) or $|\omega| \gg pn$, we can simplify expression (11) as:

$$\frac{\bar{U}}{C} = -\alpha \frac{\omega x^2}{2}. \quad (14)$$

TABLE 1
COEFFICIENTS OF $G(p, e)$ AND $H(p, e)$ TO e^4 .

p	$G(p, e)$		$H(p, e)$	
-1		$\frac{9}{4}e^2 + \frac{7}{4}e^4$		$\frac{1}{24}e^4$
-1/2		$\frac{3}{2}e + \frac{27}{16}e^3$		$\frac{1}{48}e^3$
0	1	$1 + \frac{3}{2}e^2 + \frac{15}{8}e^4$	0	
1/2		$\frac{3}{2}e + \frac{27}{16}e^3$	-	$\frac{1}{2}e + \frac{1}{16}e^3$
1		$\frac{9}{4}e^2 + \frac{7}{4}e^4$	1	$-\frac{5}{2}e^2 + \frac{13}{16}e^4$
3/2		$\frac{53}{16}e^3$		$\frac{7}{2}e - \frac{123}{16}e^3$
2		$\frac{77}{16}e^4$		$\frac{17}{2}e^2 - \frac{115}{6}e^4$
5/2				$\frac{845}{48}e^3$
3				$\frac{533}{16}e^4$

The exact expression of the coefficients is given by $G(p, e) = \frac{1}{\pi} \int_0^\pi \left(\frac{a}{r}\right)^3 \exp(i2pM) dM$ and $H(p, e) = \frac{1}{\pi} \int_0^\pi \left(\frac{a}{r}\right)^3 \exp(i2\nu) \exp(i2pM) dM$.

2.1.3. Equations of motion

The Andoyer variables (L, θ) and $(X, -\psi)$ are canonically conjugated and thus (e.g. Goldstein 1950; Kinoshita 1977)

$$\frac{dL}{dt} = -\frac{\partial \bar{U}}{\partial \theta}, \quad \frac{dX}{dt} = \frac{\partial \bar{U}}{\partial \psi}, \quad \frac{d\psi}{dt} = -\frac{\partial \bar{U}}{\partial X}. \quad (15)$$

Andoyer's variables do not give a clear view of the spin variations, despite their practical use. Since $\omega = L/C$ and $\cos \varepsilon = x = X/L$ the spin variations can be obtained as:

$$\frac{d\omega}{dt} = -\frac{\partial}{\partial \theta} \left(\frac{\bar{U}}{C} \right), \quad \frac{d\psi}{dt} = -\frac{1}{\omega} \frac{\partial}{\partial x} \left(\frac{\bar{U}}{C} \right), \quad (16)$$

and

$$\begin{aligned} \frac{dx}{dt} &= -\frac{1}{L} \left(\frac{X}{L} \frac{dL}{dt} - \frac{dX}{dt} \right) \\ &= \frac{1}{\omega} \left[x \frac{\partial}{\partial \theta} + \frac{\partial}{\partial \psi} \right] \left(\frac{\bar{U}}{C} \right). \end{aligned} \quad (17)$$

For non-resonant motion, we get from equation (14):

$$\frac{d\omega}{dt} = \frac{dx}{dt} = 0 \quad \text{and} \quad \frac{d\psi}{dt} = \alpha x. \quad (18)$$

The spin motion reduces to the precession of the spin vector about the normal to the orbital plane with rate αx .

2.2. Gravitational tides

Gravitational tides arise from differential and inelastic deformations of the planet due to the gravitational effect of a perturbing body (that can be the central star or a satellite). Tidal contributions to the planet evolution are based on a very general formulation of the tidal potential, initiated by George H. Darwin (1880). The attraction of a body with mass m_* at a distance r from the center of mass of the planet can be expressed as the gradient of a scalar potential V' , which is a sum of Legendre polynomials (e.g. Kaula 1964; Efroimsky and Williams 2009):

$$V' = \sum_{l=2}^{\infty} V'_l = -\frac{Gm_*}{r} \sum_{l=2}^{\infty} \left(\frac{r'}{r} \right)^l P_l(\cos S), \quad (19)$$

where r' is the radial distance from the planet's center, and S the angle between \mathbf{r} and \mathbf{r}' . The distortion of the planet by the potential V' gives rise to a tidal potential,

$$V_g = \sum_{l=2}^{\infty} (V_g)_l, \quad (20)$$

where $(V_g)_l = k_l V'_l$ at the planet's surface and k_l is the Love number for potential (Fig. 2). Typically, $k_2 \sim 0.25$ for Earth-like planets, and $k_2 \sim 0.40$ for giant planets (Yoder 1995). Since the tidal potential $(V_g)_l$ is an l^{th} degree harmonic, it is a solution of a Dirichlet problem, and exterior to the planet it must be proportional to r^{-l-1} (e.g.

Abramowitz and Stegun 1972; Lambeck 1980). Furthermore, as upon the surface $r' = R \ll r$, we can retain in expression (20) only the first term, $l = 2$:

$$V_g = -k_2 \frac{Gm_\star}{R} \left(\frac{R}{r}\right)^3 \left(\frac{R}{r'}\right)^3 P_2(\cos S). \quad (21)$$

In general, imperfect elasticity will cause the phase angle of V_g to lag behind that of V' (Kaula 1964) by an angle $\delta_g(\sigma)$ such that:

$$2\delta_g(\sigma) = \sigma \Delta t_g(\sigma), \quad (22)$$

$\Delta t_g(\sigma)$ being the time lag associated to the tidal frequency σ (a linear combination of the inertial rotation rate ω and the mean orbital motion n) (Fig. 3).

2.2.1. Equations of motion

Expressing the tidal potential given by expression (21) in terms of Andoyer angles (θ, ψ) , we can obtain the contribution to the spin evolution from expressions (15) using $U_g = m'V_g$ at the place of \bar{U} , where m' is the mass of the interacting body. As we are interested here in the study of the secular evolution of the spin, we also average U_g over the periods of mean anomaly and longitude of the periape of the orbit. When the interacting body is the same as the perturbing body ($m' = m_\star$), we obtain:

$$\frac{d\omega}{dt} = -\frac{Gm_\star^2 R^5}{Ca^6} \sum_{\sigma} b_g(\sigma) \Omega_{\sigma}^g(x, e), \quad (23)$$

$$\frac{d\varepsilon}{dt} = -\frac{Gm_\star^2 R^5}{Ca^6} \frac{\sin \varepsilon}{\omega} \sum_{\sigma} b_g(\sigma) \mathcal{E}_{\sigma}^g(x, e), \quad (24)$$

where the coefficients $\Omega_{\sigma}^g(x, e)$ and $\mathcal{E}_{\sigma}^g(x, e)$ are polynomials in the eccentricity (Kaula 1964). When the eccentricity is small, we can neglect the terms in e^2 , and we have:

$$\begin{aligned} \sum_{\sigma} b_{\tau}(\sigma) \Omega_{\sigma}^{\tau} &= b_{\tau}(\omega) \frac{3}{4} x^2 (1-x^2) \\ &+ b_{\tau}(\omega-2n) \frac{3}{16} (1+x)^2 (1-x^2) \\ &+ b_{\tau}(\omega+2n) \frac{3}{16} (1-x)^2 (1-x^2) \\ &+ b_{\tau}(2\omega) \frac{3}{8} (1-x^2)^2 \\ &+ b_{\tau}(2\omega-2n) \frac{3}{32} (1+x)^4 \\ &+ b_{\tau}(2\omega+2n) \frac{3}{32} (1-x)^4, \end{aligned} \quad (25)$$

and

$$\begin{aligned} \sum_{\sigma} b_{\tau}(\sigma) \mathcal{E}_{\sigma}^{\tau} &= b_{\tau}(2n) \frac{9}{16} (1-x^2) \\ &+ b_{\tau}(\omega) \frac{3}{4} x^3 \\ &- b_{\tau}(\omega-2n) \frac{3}{16} (1+x)^2 (2-x) \\ &+ b_{\tau}(\omega+2n) \frac{3}{16} (1-x)^2 (2+x) \\ &+ b_{\tau}(2\omega) \frac{3}{8} x (1-x^2) \\ &- b_{\tau}(2\omega-2n) \frac{3}{32} (1+x)^3 \\ &+ b_{\tau}(2\omega+2n) \frac{3}{32} (1-x)^3. \end{aligned} \quad (26)$$

The coefficients $b_{\tau}(\sigma)$ are related to the dissipation of the mechanical energy of tides in the planet's interior, responsible for the time delay $\Delta t_g(\sigma)$ between the position

of ‘‘maximal tide’’ and the sub-stellar point. They are related to the phase lag $\delta_g(\sigma)$ as:

$$b_g(\sigma) = k_2 \sin 2\delta_g(\sigma) = k_2 \sin(\sigma \Delta t_g(\sigma)), \quad (27)$$

where $\tau \equiv g$ for gravitational tides. Dissipation equations (23) and (24) must be invariant under the change (ω, x) by $(-\omega, -x)$ which imposes that $b(\sigma) = -b(-\sigma)$, that is, $b(\sigma)$ is an odd function of σ . Although mathematically equivalent, the couples (ω, x) and $(-\omega, -x)$ correspond to two different physical situations (Correia and Laskar 2001).

The tidal potential given by expression (21) can also be directly used to compute the orbital evolution due to tides. Indeed, it can be seen as a perturbation of the gravitational potential (Eq. 1), and the contributions to the orbit are computed using Lagrange Planetary equations (e.g. Brouwer and Clemence 1961; Kaula 1964):

$$\frac{da}{dt} = \frac{2}{\mu n a} \frac{\partial U}{\partial M}, \quad (28)$$

$$\frac{de}{dt} = \frac{\sqrt{1-e^2}}{\mu n a^2 e} \left[\sqrt{1-e^2} \frac{\partial U}{\partial M} - \frac{\partial U}{\partial \varpi} \right], \quad (29)$$

where $\mu = mm_\star/(m+m_\star) \approx m$ is the reduced mass.

We then find for the orbital evolution of the planet:

$$\frac{da}{dt} = -\frac{6Gm_\star^2 R^5}{\mu n a^7} \sum_{\sigma} b_g(\sigma) A_{\sigma}^g(x, e), \quad (30)$$

$$\frac{de}{dt} = -e \frac{3Gm_\star^2 R^5}{\mu n a^8} \sum_{\sigma} b_g(\sigma) E_{\sigma}^g(x, e), \quad (31)$$

where the coefficients $A_{\sigma}^g(x, e)$ and $E_{\sigma}^g(x, e)$ are again polynomials in the eccentricity. When the eccentricity is small, we can neglect the terms in e^2 , and we have:

$$\begin{aligned} \sum_{\sigma} b_{\tau}(\sigma) A_{\sigma}^{\tau} &= b_{\tau}(2n) \frac{9}{16} (1-x^2)^2 \\ &- b_{\tau}(\omega-2n) \frac{3}{16} (1-x^2)(1+x)^2 \\ &+ b_{\tau}(\omega+2n) \frac{3}{16} (1-x^2)(1-x)^2 \\ &- b_{\tau}(2\omega-2n) \frac{3}{32} (1+x)^4 \\ &+ b_{\tau}(2\omega+2n) \frac{3}{32} (1-x)^4, \end{aligned} \quad (32)$$

and

$$\begin{aligned} \sum_{\sigma} b_{\tau}(\sigma) E_{\sigma}^{\tau} &= b_{\tau}(n) \frac{9}{128} (5x^2-1)(7x^2-3) \\ &- b_{\tau}(2n) \frac{9}{32} (1-x^2)^2 \\ &+ b_{\tau}(3n) \frac{441}{128} (1-x^2)^2 \\ &- b_{\tau}(\omega-n) \frac{3}{64} (5x-1)(7x+1)(1-x^2) \\ &+ b_{\tau}(\omega+n) \frac{3}{64} (5x+1)(7x-1)(1-x^2) \\ &+ b_{\tau}(\omega-2n) \frac{3}{16} (1-x^2)(1+x)^2 \\ &- b_{\tau}(\omega+2n) \frac{3}{16} (1-x^2)(1-x)^2 \\ &- b_{\tau}(\omega-3n) \frac{3}{64} (1-x^2)(1+x)^2 \\ &+ b_{\tau}(\omega+3n) \frac{3}{64} (1-x^2)(1-x)^2 \\ &- b_{\tau}(2\omega-n) \frac{3}{256} (5x-7)(7x-5)(1+x)^2 \\ &+ b_{\tau}(2\omega+n) \frac{3}{256} (5x+7)(7x+5)(1-x)^2 \\ &+ b_{\tau}(2\omega-2n) \frac{3}{64} (1+x)^4 \\ &- b_{\tau}(2\omega+2n) \frac{3}{64} (1-x)^4 \\ &- b_{\tau}(2\omega-3n) \frac{147}{256} (1+x)^4 \\ &+ b_{\tau}(2\omega+3n) \frac{147}{256} (1-x)^4. \end{aligned} \quad (33)$$

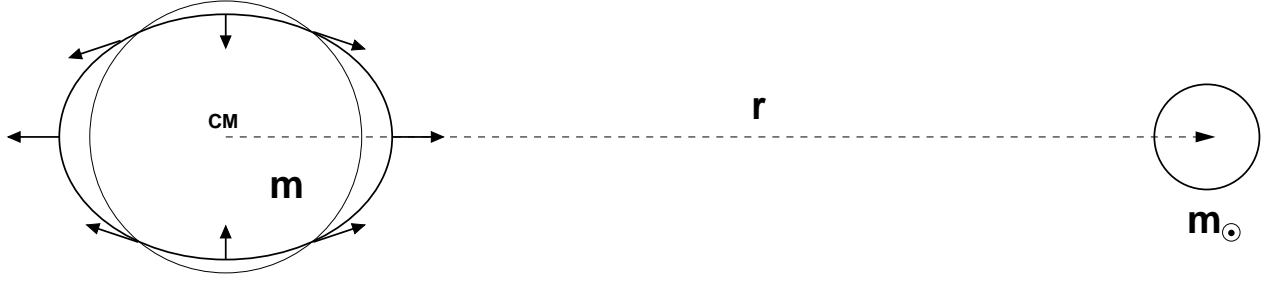


Fig. 2.— Gravitational tides. The difference between the gravitational force exerted by the mass m on a point of the surface and the center of mass is schematized by the arrows. The planet will deform following the equipotential of all present forces.

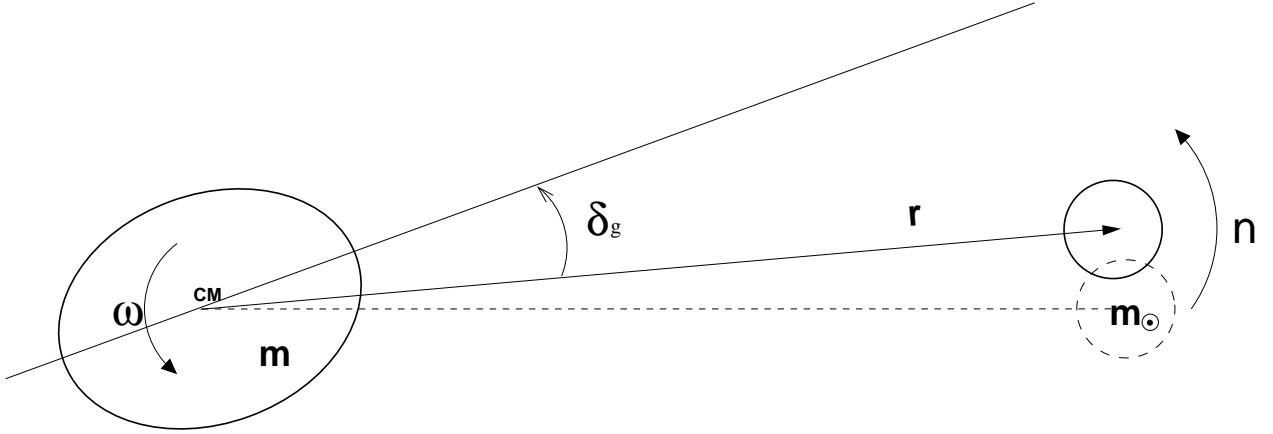


Fig. 3.— Phase lag for gravitational tides. The tidal deformation takes a delay time Δt_g to attain the equilibrium. During the time Δt_g , the planet turns by an angle $\omega \Delta t_g$ and the star by $n \Delta t_g$. For $\varepsilon = 0$, the bulge phase lag is given by $\delta_g \approx (\omega - n) \Delta t_g$.

2.2.2. Dissipation models

The dissipation of the mechanical energy of tides in the planet's interior is responsible for the phase lags $\delta(\sigma)$. A commonly used dimensionless measure of tidal damping is the quality factor Q (Munk and MacDonald 1960), defined as the inverse of the “specific” dissipation and related to the phase lags by

$$Q(\sigma) = \frac{2\pi E}{\Delta E} = \cot 2\delta(\sigma), \quad (34)$$

where E is the total tidal energy stored in the planet, and ΔE the energy dissipated per cycle. We can rewrite expression (27) as:

$$b_g(\sigma) = \frac{k_2 \text{sign}(\sigma)}{\sqrt{Q^2(\sigma) + 1}} \approx \text{sign}(\sigma) \frac{k_2}{Q(\sigma)}. \quad (35)$$

The present Q value for the planets in the Solar system can be estimated from orbital measurements, but as rheology of the planets is badly known, the exact dependence of $b_r(\sigma)$ on the tidal frequency σ is unknown. Many different authors have studied the problem and several models for $b_r(\sigma)$ have been developed so far, from the simplest ones to the more complex (for a review see Efroimsky and Williams 2009). The huge problem in validating one model better than the others is the difficulty to compare the theoretical results with the observations, as the effect of tides are very

small and can only be detected efficiently after long periods of time. Therefore, here we will only describe a few simplified models that are commonly used:

The visco-elastic model Darwin (1908) assumed that the planet behaves like a Maxwell solid, that is, the planet responds to stresses like a massless, damped harmonic oscillator. It is characterized by a rigidity (or shear modulus) μ_e and by a viscosity ν_e . A Maxwell solid behaves like an elastic solid over short time scales, but flows like a fluid over long periods of time. This behavior is also known as elasticoviscosity. For a constant density ρ , we have:

$$b_g(\sigma) = k_f \frac{\tau_b - \tau_a}{1 + (\tau_b \sigma)^2} \sigma, \quad (36)$$

where k_f is the fluid Love number (Eq. 7). $\tau_a = \nu_e / \mu_e$ and $\tau_b = \tau_a (1 + 19\mu_e R / 2Gm\rho)$ are time constants for the damping of gravitational tides.

The visco-elastic model is a realistic approximation of the planet's deformation with the tidal frequency (e.g. Escribano et al. 2008). However, when replacing expression (36) into the dynamical equations (23) and (24) we get an infinite sum of terms, which is not practical. As a consequence, simplified versions of the visco-elastic model for specific values of the tidal frequency σ are often used. For instance, when σ is small, $(\tau_b \sigma)^2$ can be neglected in

expression (36) and $b_g(\sigma)$ becomes proportional to σ .

The viscous or linear model In the viscous model, it is assumed that the response time delay to the perturbation is independent of the tidal frequency, i.e., the position of the “maximal tide” is shifted from the sub-stellar point by a constant time lag Δt_g (Mignard 1979, 1980). As usually we have $\sigma \Delta t_g \ll 1$, the viscous model becomes linear:

$$b_g(\sigma) = k_2 \sin(\sigma \Delta t_g) \approx k_2 \sigma \Delta t_g. \quad (37)$$

The viscous model is a particular case of the visco-elastic model and is specially adapted to describe the behavior of planets in slow rotating regimes ($\omega \sim n$).

The constant- Q model Since for the Earth, Q changes by less than an order of magnitude between the Chandler wobble period (about 440 days) and seismic periods of a few seconds (Munk and MacDonald 1960), it is also common to treat the specific dissipation as independent of frequency. Thus,

$$b_g(\sigma) \approx \text{sign}(\sigma) k_2 / Q. \quad (38)$$

The constant- Q model can be used for periods of time where the tidal frequency does not change much, as is the case for fast rotating planets. However, for long-term evolutions and slow rotating planets, the constant- Q model is not appropriate as it gives rise to discontinuities for $\sigma = 0$.

2.2.3. Consequences to the spin

Although both linear and constant models have some limitations, for simplicity reasons they are the most widely used in literature. The linear model has nevertheless an important advantage over the constant model: it is appropriate to describe the behavior of the planet near the equilibrium positions, since the linear model closely follows the realistic visco-elastic model for slow rotation rates. The equations of motion can also be expressed in an elegant way, so we will adopt the viscous model for the remaining of this Chapter, without loss of generality concerning the main consequences of tidal effects.

Using the approximation (37) in expressions (23) and (24), we simplify the spin equations as (Correia and Laskar 2010, Appendix B):

$$\dot{\omega} = -\frac{Kn}{C} \left(f_1(e) \frac{1 + \cos^2 \varepsilon}{2} \frac{\omega}{n} - f_2(e) \cos \varepsilon \right), \quad (39)$$

and

$$\dot{\varepsilon} \approx \frac{Kn}{C\omega} \sin \varepsilon \left(f_1(e) \cos \varepsilon \frac{\omega}{2n} - f_2(e) \right), \quad (40)$$

where

$$f_1(e) = \frac{1 + 3e^2 + 3e^4/8}{(1 - e^2)^{9/2}}, \quad (41)$$

$$f_2(e) = \frac{1 + 15e^2/2 + 45e^4/8 + 5e^6/16}{(1 - e^2)^6}, \quad (42)$$

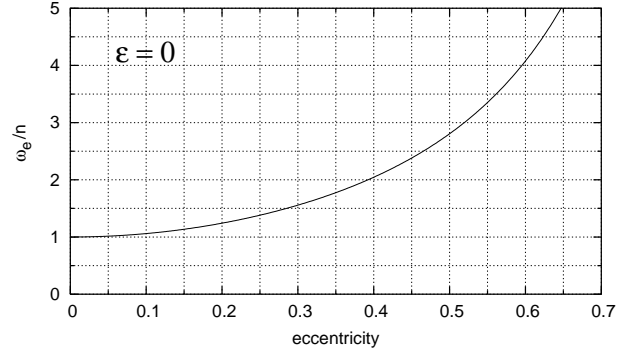


Fig. 4.— Evolution of the equilibrium rotation rate $\omega_e/n = f_2(e)/f_1(e)$ with the eccentricity when $\varepsilon = 0^\circ$ using the viscous model (Eq. 44). As the eccentricity increases, ω_e also increases. The gravitational tides lead the planet to exact resonance when the eccentricity is respectively $e_{1/1} = 0$, $e_{3/2} = 0.284926803$ and $e_{2/1} = 0.392363112$.

and

$$K = \Delta t \frac{3k_2 G m_*^2 R^5}{a^6}. \quad (43)$$

Because of the factor $1/\omega$ in the magnitude of the obliquity variations (Eq. 40), for an initial fast rotating planet the time-scale for the obliquity evolution will be longer than the time-scale for the rotation rate evolution (Eq. 39). As a consequence, it is to be expected that the rotation rate reaches an equilibrium value earlier than the obliquity. For a given obliquity and eccentricity, the equilibrium rotation rate, obtained when $\dot{\omega} = 0$, is then attained for (Fig. 4):

$$\frac{\omega_e}{n} = \frac{f_2(e)}{f_1(e)} \frac{2 \cos \varepsilon}{1 + \cos^2 \varepsilon}, \quad (44)$$

Replacing the previous equation in the expression for obliquity variations (Eq. 40), we find:

$$\dot{\varepsilon} \approx -\frac{Kn}{C\omega} f_2(e) \frac{\sin \varepsilon}{1 + \cos^2 \varepsilon}. \quad (45)$$

We then conclude that the obliquity can only decrease by tidal effect, since $\dot{\varepsilon} \leq 0$, and the final obliquity always tends to zero.

2.2.4. Consequences to the orbit

As for the spin, the semi-major axis and the eccentricity evolution can be obtained using the approximation (37) in expressions (32) and (33), respectively (Correia 2009):

$$\dot{a} = \frac{2K}{\mu a} \left(f_2(e) \cos \varepsilon \frac{\omega}{n} - f_3(e) \right), \quad (46)$$

and

$$\dot{e} = \frac{9K}{\mu a^2} \left(\frac{11}{18} f_4(e) \cos \varepsilon \frac{\omega}{n} - f_5(e) \right) e, \quad (47)$$

where

$$f_3(e) = \frac{1 + 31e^2/2 + 255e^4/8 + 185e^6/16 + 25e^8/64}{(1 - e^2)^{15/2}}, \quad (48)$$

$$f_4(e) = \frac{1 + 3e^2/2 + e^4/8}{(1 - e^2)^5}, \quad (49)$$

$$f_5(e) = \frac{1 + 15e^2/4 + 15e^4/8 + 5e^6/64}{(1 - e^2)^{13/2}}. \quad (50)$$

The ratio between orbital and spin evolution time-scales is roughly given by $C/(\mu a^2) \ll 1$, meaning that the spin achieves an equilibrium position much faster than the orbit. Replacing the equilibrium rotation rate (Eq. 44) with $\varepsilon = 0$ (for simplicity) in equations (46) and (47), gives:

$$\dot{a} = -\frac{7K}{\mu a} f_6(e) e^2, \quad (51)$$

$$\dot{e} = -\frac{7K}{2\mu a^2} f_6(e) (1 - e^2) e, \quad (52)$$

where $f_6(e) = (1 + 45e^2/14 + 8e^4 + 685e^6/224 + 255e^8/448 + 25e^{10}/1792)(1 - e^2)^{-15/2}/(1 + 3e^2 + 3e^4/8)$. Thus, we always have $\dot{a} \leq 0$ and $\dot{e} \leq 0$, and the final eccentricity is zero. Another consequence is that the quantity $a(1 - e^2)$ is conserved (Eq. 101). The final equilibrium semi-major axis is then given by

$$a_f = a(1 - e^2), \quad (53)$$

which is a natural consequence of the orbital angular momentum conservation (since the rotational angular momentum of the planet is much smaller). Notice, however, that once the equilibrium semi-major axis a_f is attained, the tidal effects on the star cannot be neglected, and they govern the future evolution of the planet's orbit.

2.3. Thermal atmospheric tides

The differential absorption of the Solar heat by the planet's atmosphere gives rise to local variations of temperature and consequently to pressure gradients. The mass of the atmosphere is then permanently redistributed, adjusting for an equilibrium position. More precisely, the particles of the atmosphere move from the high temperature zone (at the sub-stellar point) to the low temperature areas. Indeed, observations on Earth show that the pressure redistribution is essentially a superposition of two pressure waves (see Chapman and Lindzen 1970): a daily (or diurnal) tide of small amplitude (the pressure is minimal at the sub-stellar point and maximal at the antipode) and a strong half-daily (semi-diurnal) tide (the pressure is minimal at the sub-stellar point and at the antipode) (Fig. 5).

The gravitational potential generated by all of the particles in the atmosphere at a generic point of the space \mathbf{r} is given by:

$$V_a = -G \int_{(\mathcal{M})} \frac{dM}{|\mathbf{r} - \mathbf{r}'|}, \quad (54)$$

where $\mathbf{r}' = (r', \theta', \varphi')$ is the position of the atmosphere mass element dM with density $\rho_a(\mathbf{r}')$ and

$$dM = \rho_a(\mathbf{r}') r'^2 \sin \theta' dr' d\theta' d\varphi'. \quad (55)$$

Assuming that the radius of the planet is constant and that the height of the atmosphere can be neglected, we approximate expression (55) as:

$$dM = \frac{R^2}{g} p_s(\theta', \varphi', t) \sin \theta' d\theta' d\varphi', \quad (56)$$

where g is the mean surface gravity acceleration, and p_s the surface pressure, which depends on the stellar insolation. Thus, p_s depends on S , the angle between the direction of the Sun and the normal to the surface:

$$p_s(\theta', \varphi') = p_s(S) = \sum_{l=0}^{+\infty} \tilde{p}_l P_l(\cos S), \quad (57)$$

where P_l are the Legendre polynomials of order l and \tilde{p}_l its coefficients. Developing also $|\mathbf{r} - \mathbf{r}'|^{-1}$ in Legendre polynomials we rewrite expression (54) as:

$$V_a = -\frac{1}{\bar{\rho}} \sum_{l=0}^{+\infty} \frac{3}{2l+1} \tilde{p}_l \left(\frac{R}{r}\right)^{l+1} P_l(\cos S), \quad (58)$$

where $\bar{\rho}$ is the mean density of the planet. Since we are only interested in pressure oscillations, we must subtract the term of constant pressure ($l = 0$) in order to obtain the tidal potential. We also eliminate the diurnal terms ($l = 1$) because they correspond to a displacement of the center of mass of the atmosphere bulge which has no dynamical implications. Thus, since we usually have $r \gg R$, retaining only the semi-diurnal terms ($l = 2$), we write:

$$V_a = -\frac{3}{5} \frac{\tilde{p}_2}{\bar{\rho}} \left(\frac{R}{r}\right)^3 P_2(\cos S). \quad (59)$$

2.3.1. Equations of motion

Using the same methodology of previous sections, the contributions of thermal atmospheric tides to the spin evolution are obtained from expressions (15) using $U_a = m_* V_a$ at the place of \bar{U} :

$$\frac{d\omega}{dt} = -\frac{3m_* R^3}{5C \bar{\rho} a^3} \sum_{\sigma} b_a(\sigma) \Omega_{\sigma}^a(x, e), \quad (60)$$

$$\frac{d\varepsilon}{dt} = -\frac{3m_* R^3}{5C \bar{\rho} a^3} \frac{\sin \varepsilon}{\omega} \sum_{\sigma} b_a(\sigma) \mathcal{E}_{\sigma}^a(x, e), \quad (61)$$

where the terms $\Omega_{\sigma}^a(x, e)$ and $\mathcal{E}_{\sigma}^a(x, e)$ are also polynomials in the eccentricity, but different from their analogs for gravitational tides (Eqs. 23 and 24). Nevertheless, when neglecting the terms in e^2 , they become equal and are given by expressions (25) and (26), respectively (with $\tau = a$).

For thermal atmospheric tides there is also a delay before the response of the atmosphere to the excitation (Fig. 6). We name the time delay $\Delta t_a(\sigma)$ and the corresponding phase angle $\delta_a(\sigma)$ (Eq. 22). The dissipation factor $b_a(\sigma)$ is here given by:

$$b_a(\sigma) = \tilde{p}_2(\sigma) \sin 2\delta_a(\sigma) = \tilde{p}_2(\sigma) \sin(\sigma \Delta t_a(\sigma)). \quad (62)$$

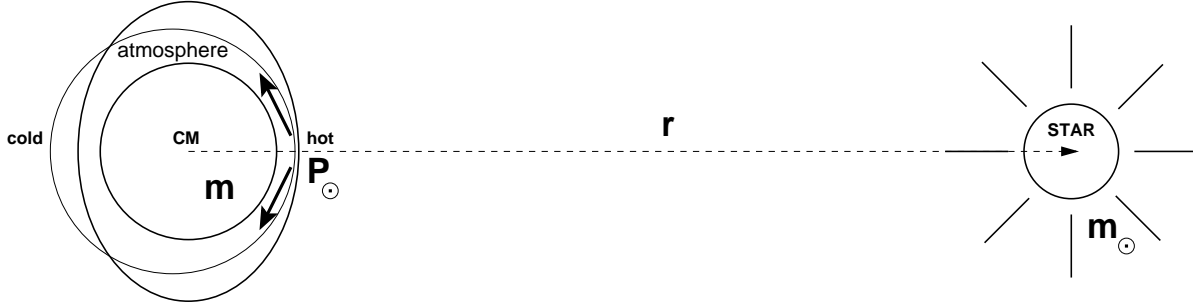


Fig. 5.— Thermal atmospheric tides. The atmosphere’s heating decreases with the distance to the sub-stellar point P_\odot . The atmospheric mass redistribution is essentially decomposed in a weak daily tide (round shape) and in a strong half-daily tide (oval shape).

Siebert (1961) and Chapman and Lindzen (1970) have shown that when

$$|\tilde{p}_2(\sigma)| \ll \tilde{p}_0, \quad (63)$$

the amplitudes of the pressure variations on the ground are given by:

$$\tilde{p}_2(\sigma) = i \frac{\gamma}{\sigma} \tilde{p}_0 \left(\nabla \cdot \mathbf{v}_\sigma - \frac{\gamma - 1}{\gamma} \frac{J_\sigma}{gH_0} \right), \quad (64)$$

where $\gamma = 7/5$ for a perfect gas, \mathbf{v} is the velocity of tidal winds, J_σ the amount of heat absorbed or emitted by a unit mass of air per unit time, and H_0 is the scale height at the surface. We can rewrite expression (64) as,

$$\begin{aligned} \tilde{p}_2(\sigma) &= \frac{\gamma}{|\sigma|} \tilde{p}_0 \left| \nabla \cdot \mathbf{v}_\sigma - \frac{\gamma - 1}{\gamma} \frac{J_\sigma}{gH_0} \right| e^{\pm i \frac{\pi}{2}} \\ &= |\tilde{p}_2(\sigma)| e^{\pm i \frac{\pi}{2}}, \end{aligned} \quad (65)$$

where the factor $e^{\pm i \frac{\pi}{2}}$ can be seen as a supplementary phase lag of $\pm \pi/2$:

$$\begin{aligned} b_a(\sigma) &= |\tilde{p}_2(\sigma)| \sin 2 \left(\delta_a(\sigma) \pm \frac{\pi}{2} \right) \\ &= -|\tilde{p}_2(\sigma)| \sin 2\delta_a(\sigma). \end{aligned} \quad (66)$$

The minus sign above causes pressure variations to lead the Sun whenever $\delta_a(\sigma) < \pi/2$ (Chapman and Lindzen 1970; Dobrovolskis and Ingersoll 1980) (Fig. 6).

2.3.2. Dissipation models

Unfortunately, our knowledge of the atmosphere response to thermal excitation is still very incomplete. As for the gravitational tides, models are developed to deal with the unknown part. Dobrovolskis and Ingersoll (1980) adopted a model called “*heating at the ground*”, where they suppose that all the stellar flux absorbed by the ground F_s is immediately deposited in a thin layer of atmosphere at the surface. The heating distributing may then be written as a delta-function just above the ground:

$$J(r) = \frac{g}{\tilde{p}_0} F_s \delta(r - 0^+). \quad (67)$$

Neglecting \mathbf{v} over the thin heated layer, expression (64) simplifies:

$$|\tilde{p}_2(\sigma)| = \frac{5}{16} \frac{\gamma - 1}{|\sigma|} \frac{F_s}{H_0} = \frac{5}{16} \frac{\gamma}{|\sigma|} \frac{gF_s}{c_p \bar{T}_s}, \quad (68)$$

where the factor $5/16$ represents the second-degree harmonic component of the insolation contribution (Dobrovolskis and Ingersoll 1980) and c_p is the specific heat at constant pressure.

Nevertheless, according to expression (68), if $\sigma = 0$, the amplitude of the pressure variations $\tilde{p}_2(\sigma)$ becomes infinite. The amplitude cannot grow infinitely, as for a tidal frequency equal to zero, a steady distribution is attained, and thus $\tilde{p}_2(0) = 0$. Indeed, expression (64) is not valid when $\sigma \approx 0$ because the condition (63) is no longer verified. Using the typically accepted values for the Venusian atmosphere, $c_p \approx 1000 \text{ K kg}^{-1} \text{ s}^{-1}$, $\bar{T}_s \approx 730 \text{ K}$ and $F_s \approx 100 \text{ W m}^{-2}$ (Avduevskii et al. 1976) we compute:

$$|\tilde{p}_2(\sigma)| \approx 10^{-4} \tilde{p}_0 \frac{n}{|\sigma|}, \quad (69)$$

which means that for $\sigma \sim n$, the “*heating at the ground*” model of Dobrovolskis and Ingersoll (1980), can still be applied. Since we are only interested in long-term behaviors we can set $\tilde{p}_2(\sigma) = 0$ whenever $|\sigma| \ll n/100$. Moreover, for tidal frequencies $\sigma \sim 0$ the dissipation lag $\sin(\sigma \Delta t_a(\sigma)) \approx \sigma \Delta t_a(\sigma)$ also goes to zero. We expect that further studies about synchronous exoplanets’ atmospheres (e.g. Joshi et al. 1997; Arras and Socrates 2010), may provide a more accurate solution for the case $\sigma \approx 0$.

In presence of a dense atmosphere, another kind of tides can arise: the atmosphere pressure upon the surface gives rise to a deformation, a pressure bulge, that will also be affected by the stellar torque. At the same time, the atmosphere itself exerts a torque over the planet’s bulges (gravitational and pressure bulge). Nevertheless, we do not need to take into account additional tidal effects as their consequences upon the dynamical equations can be neglected (Hinderer et al. 1987; Correia and Laskar 2003a).

2.4. Spin-orbit resonances

A spin-orbit resonance occurs when there is a commensurability between the rotation rate ω and the mean motion

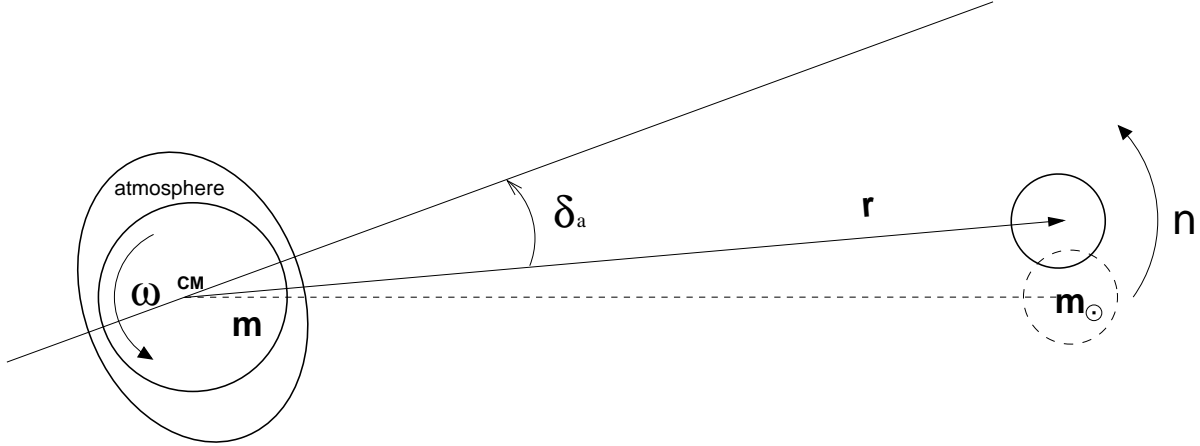


Fig. 6.— Phase lag for thermal atmospheric tides. During the time Δt_a the planet turns by an angle $\omega\Delta t_a$ and the star by $n\Delta t_a$. For $\varepsilon = 0$, the bulge phase lag is given by $\delta_a \approx (\omega - n)\Delta t_a$.

of the orbit n (Eqs. 9 and 10). The synchronous rotation of the Moon is the most common example. After the discovery of the $3/2$ spin-orbit resonance of Mercury (Colombo 1965), spin-orbit resonances were studied in great detail (Colombo and Shapiro 1966; Goldreich and Peale 1966; Counselman and Shapiro 1970; Correia and Laskar 2004, 2009, 2010). When resonant motion is present we cannot neglect the terms in β in expression (11). Assuming for simplicity a low obliquity ($x \approx 1$) we obtain a non-zero contribution for the rotation rate (Eq. 16):

$$\frac{d\omega}{dt} = -\beta H(p, e) \sin 2\gamma, \quad (70)$$

where $\gamma = \theta - pM - \phi$. The rotation of the planet will therefore present oscillations around a mean value. The width of the corresponding resonance, centered at $\omega = pn$, is:

$$\Delta\omega = \sqrt{2\beta H(p, e)}. \quad (71)$$

Due to the tidal torque (Eq. 23), here denoted by \bar{T} , the mean rotation rate does not remain constant and may therefore cross and be captured in a spin-orbit resonance. Goldreich and Peale (1966) computed a simple estimation of the capture probability P_{cap} , and subsequent more detailed studies proved their expression to be essentially correct (for a review, see Henrard 1993). Since the tidal torques can usually be described by means of the torques considered by Goldreich and Peale (1966), we will adopt here the same notations. Let

$$\bar{T} = -K \left(V + \frac{\dot{\gamma}}{n} \right), \quad (72)$$

where K and V are positive constant torques, and $\dot{\gamma} = \omega - pn$. The probability of capture into resonance is then given by (Goldreich and Peale 1966):

$$P_{\text{cap}} = \frac{2}{1 + \pi V n / \Delta\omega}, \quad (73)$$

where $\Delta\omega$ is the resonance width (Eq. 71). In the slow rotation regime ($\omega \sim n$), where the spin encounters spin-orbit resonances and capture may occur, we compute for the viscous tidal model (Eq. 39):

$$P_{\text{cap}} = 2 \left[1 + \left(p - \frac{2x}{1+x^2} \frac{f_2(e)}{f_1(e)} \right) \frac{n\pi}{2\Delta\omega} \right]^{-1}, \quad (74)$$

2.5. Planetary perturbations

Like in the Solar System, many exoplanets are not alone in their orbits, but belong to multi-planet systems. Because of mutual planetary perturbations the orbital parameters of the planets do not remain constant and undergo secular variations in time (Chapter 10: *Non-Keplerian Dynamics*). An important consequence for the spin of the planets is that the reference orbital plane (to which the obliquity and the precession were defined) will also present variations. We can track the orbital plane variations by the inclination to an inertial reference plane, I , and by the longitude of the line of nodes, Ω . Under the assumption of principal axis rotation, the energy perturbation attached to an inertial frame can be written (Kinoshita 1977; Néron de Surgy and Laskar 1997):

$$U_{pp} = [X(1 - \cos I) - L \sin \varepsilon \sin I \cos \varphi] \frac{d\Omega}{dt} + L \sin \varepsilon \sin \varphi \frac{dI}{dt}, \quad (75)$$

where $\varphi = -\Omega - \psi$.

Although the Solar System motion is chaotic (Laskar 1989, 1990), the motion can be approximated over several million of years by quasi-periodic series. In particular for the orbital elements that are involved in the precession driving terms (Eq. 75), we have (Laskar and Robutel 1993):

$$\left(\frac{dI}{dt} + i \frac{d\Omega}{dt} \sin I \right) e^{i\Omega} = \sum_k \mathcal{J}_k e^{i(\nu_k t + \phi_k)}, \quad (76)$$

and

$$(1 - \cos I) \frac{d\Omega}{dt} = \sum_k \mathcal{L}_k \cos(\nu_k t + \varphi_k), \quad (77)$$

where ν_k are secular frequencies of the orbital motion with amplitude \mathcal{J}_k and phase ϕ_k , and $i = \sqrt{-1}$. We may then rewrite expression (75) as

$$U_{pp} = L \sum_k \left[\mathcal{L}_k \cos(\nu_k t + \varphi_k) x - \mathcal{J}_k \sqrt{1 - x^2} \sin(\nu_k t + \psi + \phi_k) \right]. \quad (78)$$

Assuming non-resonant motion, from equations (16) and (17) we get for the spin motion:

$$\frac{d\varepsilon}{dt} = \sum_k \mathcal{J}_k \cos(\nu_k t + \psi + \phi_k), \quad (79)$$

and

$$\frac{d\psi}{dt} = \alpha \cos \varepsilon - \sum_k \mathcal{L}_k \cos(\nu_k t + \varphi_k) - \cot \varepsilon \sum_k \mathcal{J}_k \sin(\nu_k t + \psi + \phi_k). \quad (80)$$

For planetary systems like the Solar System, the mutual inclinations remain small (Laskar 1990; Correia et al. 2010), and it follows from expressions (76) and (77) that the amplitudes of \mathcal{J}_k and \mathcal{L}_k are bounded respectively by

$$\mathcal{J}_k \sim \nu_k I_{max}, \quad \mathcal{L}_k \sim \nu_k I_{max}^2 / 2. \quad (81)$$

The term in \mathcal{L}_k in expression (80) for the precession variations can then be neglected for small inclinations.

From expression (79) it is clear that a resonance can occur whenever the precession frequency is equal to the opposite of a secular frequency ν_k (that is, $\dot{\psi} = -\nu_k$). Retaining only the terms in k , the problem becomes integrable. We can search for the equilibrium positions by setting the obliquity variations equal to zero ($\dot{\varepsilon} = 0$). It follows then from expression (79) that $\psi + \nu_k t + \phi_k = \pm\pi/2$, and replacing it in expression (80) with $\dot{\psi} = -\nu_k$, we get

$$\alpha \cos \varepsilon \sin \varepsilon + \nu_k \sin \varepsilon \approx \mathcal{J}_k \cos \varepsilon, \quad (82)$$

which gives the equilibrium positions for the spin of the planet, generally known as ‘‘Cassini states’’ (e.g. Henrard and Murigande 1987). Since $\mathcal{J}_k/\nu_k \ll 1$ (Eq. 81), the equilibrium positions for the obliquity are then:

$$\tan \varepsilon \approx \frac{\mathcal{J}_k}{\nu_k \pm \alpha}, \quad \cos \varepsilon \approx -\frac{\nu_k}{\alpha}. \quad (83)$$

When $|\alpha/\nu_k| \ll |\alpha/\nu_{crit}|$, the first expression gives states 2 and 3, while the second expression has no real roots (states 1 and 4 do not exist). When $|\alpha/\nu_k| \gg |\alpha/\nu_{crit}|$, the first

expression approximates Cassini states 1 and 3, while the second one gives states 2 and 4. States 1, 2 and 3 are stable, while state 4 is unstable. Although gravitational tides always decrease the obliquity (Eq. 45), the ultimate stage of the obliquity evolution is to be captured into a Cassini resonant state, similarly to the capture of the rotation in a spin-orbit resonance (Eq. 73).

The complete system (Eqs. 79 and 80) is usually not integrable as there are several terms in expression (76), but we can look individually to the location of each resonance. When the resonances are far apart, the motion will behave locally as in the integrable case, with just the addition of supplementary small oscillations. However, if several resonances overlap, the motion is no longer regular and becomes chaotic (Chirikov 1979; Laskar 1996). For instance, the present obliquity variations on Mars are chaotic and can vary from zero to nearly sixty degrees (Laskar and Robutel 1993; Touma and Wisdom 1993; Laskar et al. 2004b).

3. APPLICATION TO THE PLANETS

The orbital parameters of exoplanets are reasonably well determined from radial velocity, transit or astrometry techniques, but exoplanets’ spins remain a mystery.

The same applies to the primordial spins of the terrestrial planets in the Solar System, since very little constraints can be derived from the present planetary formation models. Indeed, a small number of large impacts at the end of the formation process will not average, and can change the spin direction. The angular velocities are also unpredictable, but they are usually high, $\omega \gg n$ (Dones and Tremaine 1993; Agnor et al. 1999; Kokubo and Ida 2007), although impacts can also form a slow rotating planet ($\omega \sim n$) if the size of the typical accreting bodies is much smaller than the protoplanet (e.g. Schlichting and Sari 2007). The critical angular velocity for rotational instability is Kokubo and Ida (2007):

$$\omega_{cr} \approx 3.3 \left(\frac{\rho}{3 \text{ g cm}^{-3}} \right)^{1/2} \text{ hr}^{-1}, \quad (84)$$

which sets a maximum initial rotation periods of about 1.4 h, for the inner planets of the Solar System.

For the Jovian planets in the Solar System no important mechanism susceptible of altering the rotation rate is known, but the orientation of the axis may also change by secular resonance with the planets (e.g. Correia and Laskar 2003b; Ward and Hamilton 2004; Boué and Laskar 2010). The fact that all Jovian planets rotate fast (Table 3) seems to be in agreement with theoretical predictions (e.g. Takata and Stevenson 1996).

An empirical relation derived by MacDonald (1964) based on the present rotation rates of planets from Mars to Neptune (assumed almost unchanged) gives for the initial rotation rates

$$\omega_0 \propto m^{4/5} R^{-2}. \quad (85)$$

Extrapolating for the remaining inner planets, we get initial rotation periods of about 18.9 h, 13.5 h, and 12.7 h for Mercury, Venus and the Earth, respectively, much faster than

today’s values, which in agreement with the present formation theories.

The above considerations and expressions can also be extended to exoplanets. However, since many of the exoplanets are close to their host stars, it is believed that the spins have undergone significant tidal dissipation and eventually reached some equilibrium positions, as it happens for Mercury and Venus in the Solar System. Therefore, in this section we will first review the rotation of the terrestrial planets, and then look at the already known exoplanets. In particular, we will focus our attention in two classes of exoplanets, the “Hot-Jupiters” (fluid) and the “Super-Earths” (rocky with atmosphere), for which tidal effects may play an important role in orbital and spin evolution.

3.1. Solar System examples

3.1.1. Mercury

The present spin of Mercury is very peculiar: the planet rotates three times around its axis in the same time as it completes two orbital revolutions (Pettengill and Dyce 1965). Within a year of the discovery, the stability of this 3/2 spin-orbit resonance became understood as the result of the solar torque on Mercury’s quadrupolar moment of inertia combined with an eccentric orbit (Eq. 70) (Colombo and Shapiro 1966; Goldreich and Peale 1966). The way the planet evolved into the 3/2 configuration remained a mystery for long time, but can be explained as the result of tidal evolution combined with the eccentricity variations due to planetary perturbations (Correia and Laskar 2004, 2009).

Mercury has no atmosphere, and the spin evolution of the planet is therefore controlled by gravitational tidal interactions with the Sun. Tidal effects drive the final obliquity of Mercury close to zero (Eq. 45), and the averaged equation for the rotation motion near the p resonance can be written putting expressions (70) and (39) together:

$$\frac{d\omega}{dt} = -\beta' \sin 2\gamma - K' \left[\frac{\omega}{n} - \frac{f_2(e)}{f_1(e)} \right], \quad (86)$$

where $\gamma = \theta - pM - \phi$, $\beta' = \beta H(p, e)$, and $K' = Knf_1(e)/C$. Note that near the p resonance a contribution from core-mantle friction may also be present, but we will neglect it here (for a full description see Correia and Laskar 2009, 2010). The tidal equilibrium is achieved when $d\omega/dt = 0$, that is, for a constant eccentricity e , when $\omega/n = f_2(e)/f_1(e)$. In a circular orbit ($e = 0$) the tidal equilibrium coincides with synchronization, while the equilibrium rotation rate $\omega/n = 3/2$ is achieved for $e_{3/2} = 0.284927$ (Fig. 4).

For the present value of Mercury’s eccentricity ($e \approx 0.206$), the capture probability in the 3/2 spin-orbit resonance is only about 7% (Eq. 74). However, as the eccentricity of Mercury suffers strong chaotic variations in time due to planetary secular perturbations, the eccentricity can vary from nearly zero to more than 0.45, and thus reach values higher than the critical value $e_{3/2} = 0.284927$. Additional

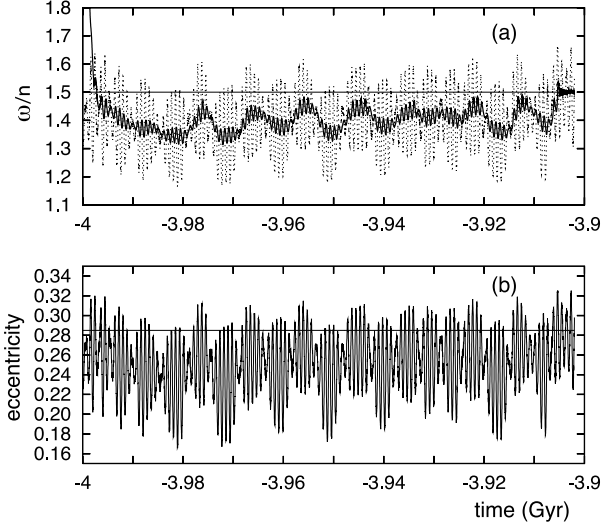


Fig. 7.— Simultaneous evolution of the rotation rate (a) and the eccentricity (b) of Mercury. In this example, there is no capture at the first encounter with the 3/2 resonance (at $t \approx -3.9974$ Gyr). About 100 Myr later, as the mean eccentricity increases, additional crossing of the 3/2 resonance occurs, leading to capture with damping of the libration (Correia and Laskar 2006).

capture into resonance can then occur, at any time during the planet’s history (Correia and Laskar 2004).

In order to check the past evolution of Mercury’s spin, it is not possible to use a single orbital solution, as due to the chaotic behavior the motion cannot be predicted precisely beyond a few tens of millions of years. A statistical study of the past evolutions of Mercury’s orbit was then performed, with the integration of 1000 orbits over 4 Gyr in the past, starting with very close initial conditions, within the uncertainty of the present determinations (Correia and Laskar 2004, 2009).

For each of the 1000 orbital motion of Mercury, the rotational motion (Eq. 86) was integrated numerically with planetary perturbations. As $e(t)$ is not constant, $\omega(t)$ will tend towards a limit value $\tilde{\omega}(t)$ that is similar to an averaged value of $(f_2/f_1)(e(t))$ and capture into resonance can now occur more often (Fig. 7). Globally, only 38.8% of the solutions did not end into resonance, and the final capture probability distribution was (Correia and Laskar 2004):

$$P_{1/1} = 2.2\%, \quad P_{3/2} = 55.4\%, \quad P_{2/1} = 3.6\%.$$

With the consideration of the chaotic evolution of the eccentricity of Mercury, the present 3/2 resonant state becomes the most probable outcome for the spin evolution. The largest unknown remains the dissipation factor $k_2\Delta t$ in the expression of K (Eq. 43). A stronger dissipation increases the probability of capture into the 3/2 resonance, as ω/n would follow more closely $f_2(e)/f_1(e)$ (Fig. 7), while lower dissipation slightly decreases the capture probability. The inclusion of core-mantle friction also increases the chances of capture for all resonances (Correia and Laskar 2009, 2010).

TABLE 2
POSSIBLE FINAL SPIN STATES OF VENUS.

state	ε	ω	P (days)	P_s (days)
F_0^+	0°	$n + \omega_s$	76.83	116.75
F_0^-	0°	$n - \omega_s$	-243.02	-116.75
F_π^+	180°	$-n - \omega_s$	-76.83	116.75
F_π^-	180°	$-n + \omega_s$	243.02	-116.75

There are two retrograde states (F_0^- and F_π^-) and two prograde states (F_0^+ and F_π^+). In all cases the synodic period P_s is the same (Correia and Laskar 2001).

3.1.2. Venus

Venus is a unique case in the Solar System: it presents a slow retrograde rotation, with an obliquity close to 180 degrees and a 243-day period (Smith 1963; Goldstein 1964; Carpenter 1970). According to planetary formation theories it is highly improbable that the present spin of Venus is primordial, since we would expect a lower obliquity and a fast rotating planet (Eq. 85).

The present rotation of Venus is believed to represent a steady state resulting from a balance between gravitational tides, which drives the planet toward synchronous rotation, and thermally driven atmospheric tides, which drives the rotation away (e.g. Gold and Soter 1969). The conjugated effect of tides and core-mantle friction can tilt Venus down during the planet past evolution, but requires high values of the initial obliquity (e.g. Dobrovolskis 1980; Yoder 1997). However, the crossing in the past of a large chaotic zone for the spin, resulting from secular planetary perturbations (Laskar and Robutel 1993), can lead Venus to the present retrograde configuration for most initial conditions (Correia and Laskar 2001, 2003b).

Venus has a dense atmosphere and the planet is also enough close to the Sun to undergo significant tidal dissipation. Venus' spin evolution is then controlled by tidal effects (both gravitational and thermal). Tidal effects combined can drive the obliquity either to $\varepsilon = 0^\circ$ or $\varepsilon = 180^\circ$ (Correia et al. 2003). For the two final obliquity possibilities, the tidal components become very simplified, with (at second order in the planetary eccentricity) a single term of tidal frequency $\sigma = 2\omega - 2n$ for $\varepsilon = 0$ and $\sigma = 2\omega + 2n$ for $\varepsilon = \pi$ (Eq. 25). Combining expressions (23) and (60) we can write for the rotation rate:

$$\begin{aligned} \left. \frac{d\omega}{dt} \right|_0 &= -\frac{3}{2} [K_g b_g (2\omega - 2n) + K_a b_a (2\omega - 2n)], \\ \left. \frac{d\omega}{dt} \right|_\pi &= -\frac{3}{2} [K_g b_g (2\omega + 2n) + K_a b_a (2\omega + 2n)], \end{aligned} \quad (87)$$

where K_g and K_a are given by the constant part of expres-

sions (23) and (60), respectively. Let $f(\sigma)$ be defined as

$$f(\sigma) = \frac{b_a(2\sigma)}{b_g(2\sigma)}. \quad (88)$$

As $b_\tau(\sigma)$ is an odd function of σ (Eq. 25), $f(\sigma)$ is an even function of σ of the form $f(|\sigma|)$. Thus, at equilibrium, with $d\omega/dt = 0$, we obtain an equilibrium condition

$$f(|\omega - xn|) = -\frac{K_g}{K_a}, \quad (89)$$

where $x = +1$ for $\varepsilon = 0$ and $x = -1$ for $\varepsilon = \pi$. Moreover, for all commonly used dissipation models f is monotonic and decreasing for slow rotation rates. There are thus only four possible values for the final rotation rate ω_f of Venus, given by

$$|\omega_f - xn| = f^{-1}\left(-\frac{K_g}{K_a}\right) = \omega_s. \quad (90)$$

Assuming that the present rotation of Venus corresponds to a stable retrograde rotation, since $\omega_s > 0$ the only possibilities for the present rotation are $\varepsilon = 0$ and $\omega_{obs} = n - \omega_s$, or $\varepsilon = \pi$ and $\omega_{obs} = \omega_s - n$. In both cases, $\omega_s = n + |\omega_{obs}|$ (ω_s is thus the synodic frequency). With

$$\omega_{obs} = 2\pi/243.0185 \text{ day}; \quad n = 2\pi/224.701 \text{ day}, \quad (91)$$

we have

$$\omega_s = 2\pi/116.751 \text{ day}. \quad (92)$$

We can then determine all four final states for Venus (Table 2). There are two retrograde states (F_0^- and F_π^-) and two prograde states (F_0^+ and F_π^+). The two retrograde states correspond to the observed present retrograde state of Venus with period 243.02 days, while the two other states have a prograde rotation period of 76.83 days. Looking to the present rotation state of the planet, it is impossible to distinguish between the two states with the same angular momentum (Fig. 8).

In order to obtain a global view of the possible final evolutions of Venus' spin, numerical integrations of the equations of motion for the dissipative effects (Eqs. 23, 24,

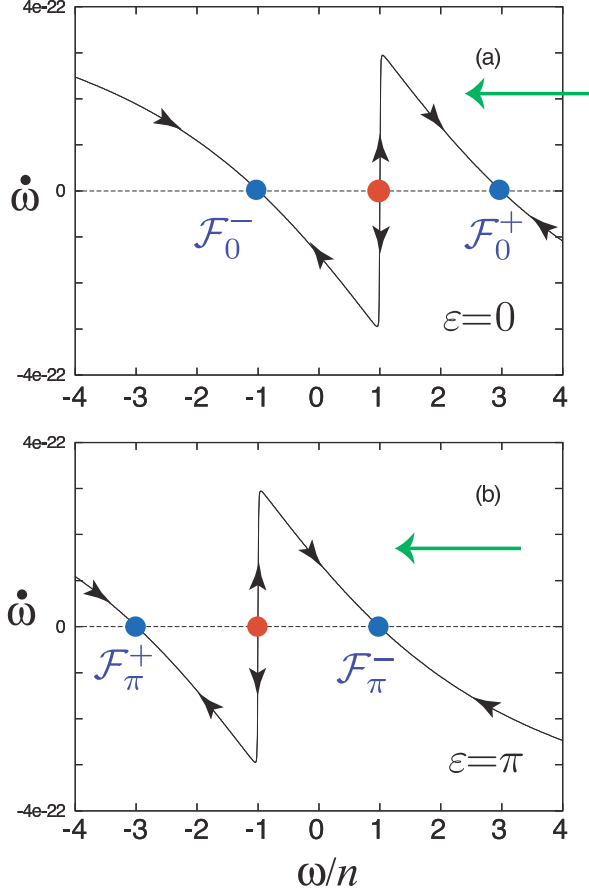


Fig. 8.— Final states for a planet with strong atmospheric thermal tides. The original equilibrium point obtained at synchronization ($\omega/n = 1$) when considering uniquely the gravitational tides, becomes unstable, and bifurcates at $\epsilon = 0$ into two new stable fixed points F_0^- and F_0^+ , and at $\epsilon = \pi$ into F_π^- and F_π^+ (Correia and Laskar 2001, 2003b).

60 and 61), with the addition of planetary perturbations (Eqs. 79 and 80) were performed (Correia and Laskar 2001, 2003b). In Figure 9 we show the possible final evolutions for a planet starting with an initial period ranging from 3 to 12 days, with an increment of 0.25 day, and initial obliquity from 0° to 180° , with an increment of 2.5 degrees (rotation periods faster than 3 days are excluded as they do not allow the planet to reach a final rotation state within the age of the Solar System). Each color represents one of the possible final states. For high initial obliquities, the spin of Venus always evolves into the retrograde final state F_π^- . It is essentially the same evolution as without planetary perturbations, since none of the trajectories encounters a chaotic zone for the obliquity (Laskar and Robutel 1993). However, for evolutionary paths starting with low initial obliquities, we can distinguish two different zones: one zone corresponding to slow initial rotation periods ($P_i > 8$ day) where the prograde rotation final state F_0^- is prevailing, and another zone for faster initial rotation periods ($P_i < 8$ day), where we find a mixture of the three attainable final states, F_0^+ , F_0^- and F_π^- . To emphasize the chaotic behavior, we integrated

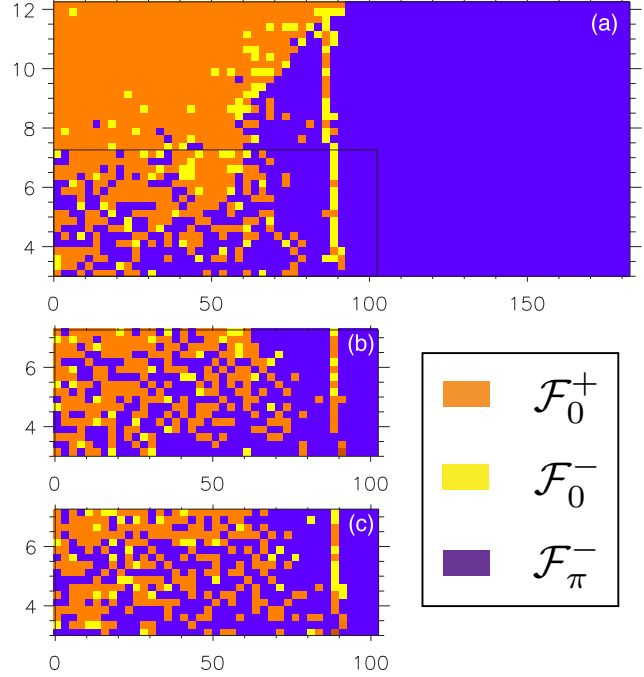


Fig. 9.— Final states of Venus' spin with planetary perturbations for initial obliquity ($\epsilon_i \in [0^\circ, 180^\circ]$) and period ($P_i \in [3 \text{ d}, 12 \text{ d}]$). For high initial obliquities, the final evolution of Venus remains essentially unchanged since none of the trajectories crossed the chaotic zone. The passage through the chaotic zone is reflected by the scattering of the final states in the left side of the picture. To emphasize the chaotic behavior, in the bottom left corner of picture (a), additional integrations were done with the same initial conditions, but with a difference of 10^{-9} in the initial eccentricity of Mars (b) and Neptune (c) (Correia and Laskar 2003b).

twice more the zone with $P_i < 8$ day, with a difference of 10^{-9} in the initial eccentricity of Mars (Fig. 9b), and with a difference of 10^{-9} in the initial eccentricity of Neptune (Fig. 9c). The passage through the chaotic zone is reflected by the scattering of the final states in the left hand side of the picture.

3.1.3. The Earth and Mars

Contrary to Mercury and Venus, the Earth and Mars are not tidally evolved. For Mars, the tidal dissipation from the Sun is negligible. For the Earth, tidal dissipation is noticeable due to the presence of the Moon, but the Earth's spin is still far from the equilibrium (e.g. Néron de Surgy and Laskar 1997). Nevertheless, the spin axis of both planets is subjected to planetary perturbations and thus present some significant variations (Sect. 2.5).

In the case of Mars, the presence of numerous secular resonances of the kind $\dot{\psi} = -\nu_k$ (Eq. 79) induce large chaotic variations in the obliquity, which can evolve between 0 and 60 degrees (Fig. 10). At present, the obliquity of Mars is very similar to the obliquity of the Earth, which is a mere coincidence. Indeed, the obliquity of Mars has most certainly reached values larger than 45 degrees in the past (Laskar et al. 2004a). The high obliquity periods led to

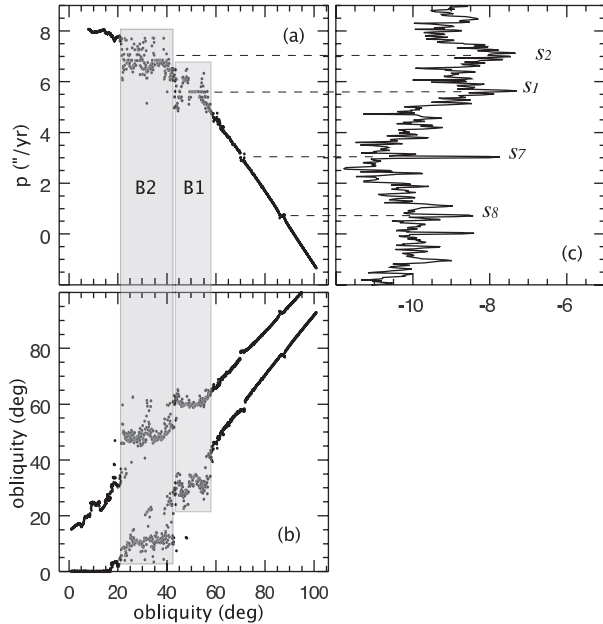


Fig. 10.— Frequency analysis of Mars’ obliquity. (a) The frequency map is obtained by reporting in the ordinate the precession frequency value obtained for 1000 integrations over 56 Myr for the different values of the initial obliquity (abscissa). A large chaotic zone is visible, ranging from 0° to about 60° , with two distinct chaotic zones, *B1* and *B2*. (b) Maximum and minimum values of the obliquity reached over 56 Myr. In (c), the power spectrum of the orbital forcing term (Eq. 76) is given in logarithmic scale, showing the correspondence of the chaotic zone with the main secular frequencies s_1, s_2, s_7, s_8 . (Laskar et al. 2004a).

large climatic changes on Mars, with possible occurrence of large scale ice cycles where the polar caps are sublimated during high obliquity stages and the ice is deposited in the equatorial regions (Laskar et al. 2002; Levrard et al. 2004, 2007b).

In the case of the Earth, the precession frequency is not in resonance with any orbital secular frequency ($\psi \neq \nu_k$). The obliquity of the Earth is then only subject to small oscillations of about 1.3 degrees around the mean value (23.3 degrees) with main periodicities around 40 000 years (Laskar et al. 2004b). The small obliquity variations are nevertheless sufficiently important to induce substantial changes in the insolation received in summer in high latitude regions on the Earth, and they are imprinted in the geological stratigraphic sequences (Hays et al. 1976; Imbrie 1982).

Due to tidal dissipation in the Earth-Moon system, the Moon is moving away from Earth at a 3.8 cm/yr rate (Dickey et al. 1994), and the rotation rate of the Earth is slowing down (Eqs. 46 and 39, respectively). As a consequence, the torque exerted on the equatorial bulge of the Earth decreases and thus also the Earth precession frequency (Eqs. 7 and 12). Using the present dissipation parameters of the Earth, Néron de Surgy and Laskar (1997) found that after 1.5 Gyr, the spin of the Earth will enter

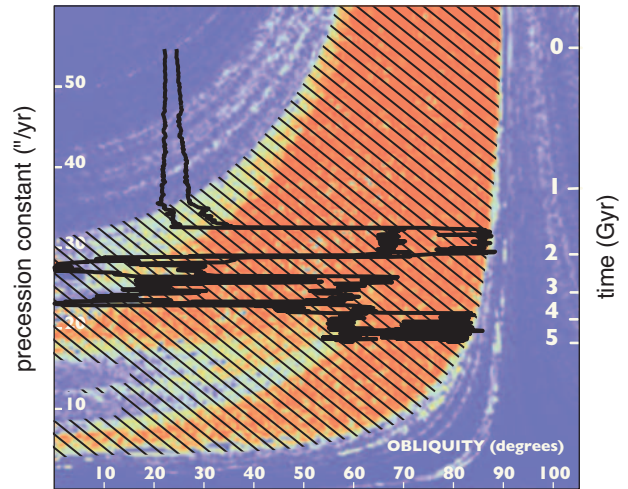


Fig. 11.— Example of possible evolution of the Earth’s obliquity for 5 Gyr in the future, due to tidal dissipation in the Earth-Moon system. The background of the figure is obtained as the result of a stability analysis on about 250 000 numerical integrations of the obliquity of the Earth under planetary perturbations for 36 Myr, for various values of the initial obliquity of the Earth (x -axis) and various values of the precession constant (left y -axis). We observe a very large chaotic zone (with stripes on the figure) resulting from overlap of orbital secular resonances (Laskar et al. 1993; Laskar and Robutel 1993). The numerical integration is then conducted over 5 Gyr years in the future for the obliquity of the Earth, including tidal dissipative effects. The two bold curves correspond to the minimum and maximum values reached by the obliquity and the time scale is given in the right y -axis. As long as the orbits stays in the regular region, the motion suffers only small (and regular) variations. As soon as the orbit enters the chaotic zone, very strong variations of the obliquity are observed, which wanders in all the chaotic zone, and very high values, close to 90 degrees, are reached (Néron de Surgy and Laskar 1997).

a large chaotic zone of overlapping orbital secular resonances. From then, the Earth spin axis will evolve in a wildly chaotic way, with a possible range from 0 to nearly 90 degrees (Fig. 11).

The main difference between the Earth and Mars is thus due to the presence of the Moon, whose gravitational torque on the equatorial bulge of the Earth prevents the spin axis to evolve in a largely chaotic state. In absence of the Moon, the behavior of the spin axis of the Earth and Mars would be identical (Laskar et al. 1993; Laskar and Robutel 1993).

Depending on the orbital configuration of the exoplanetary systems, we thus expect to find planets that would be either in a chaotic state as Mars or the moonless Earth, or in a regular state as the Earth with the Moon. It should be stressed, however, the presence of a large satellite is not mandatory in order to stabilize the spin axis. Since the stability of the axis is very important for the exoplanet climate, planetary perturbations should be taken into consideration when searching for another Earth-like environments.

TABLE 3
CONSTANTS FOR THE SOLAR SYSTEM OUTER PLANETS.

quantity	Jupiter	Saturn	Uranus	Neptune
P_0 (h)	9.92	10.66	17.24	16.11
ρ (g/cm ³)	1.33	0.69	1.32	1.64
C/MR^2	0.25	0.21	0.23	0.24
k_2	0.49	0.32	0.36	0.41
Q ($\times 10^4$)	~ 3	~ 2	1 \sim 3	1 \sim 30

(Yoder 1995; Veeder et al. 1994; Dermott et al. 1988; Tittlemore and Wisdom 1990; Banfield and Murray 1992).

3.2. “Hot-Jupiters”

One of the most surprising findings concerning exoplanets was the discovery of several giant planets with periods down to 3 days, that were designated by “Hot-Jupiters” (e.g. Santos et al. 2005). Many of the “Hot-Jupiters” were simultaneously detected by transit method and radial Doppler shift, which allows the direct and accurate determination of both mass and radius of the exoplanet. Therefore, “Hot-Jupiters” are amongst the better characterized planets outside the Solar System.

Due to the proximity of the host star, “Hot-Jupiters” are almost certainly tidally evolved. Given the large mass of “Hot-Jupiters”, they may essentially be composed of an extensive Hydrogen atmosphere, similar to Jupiter or Saturn. As a consequence, despite the presence of an inner metallic core, “Hot-Jupiters” can be treated as fluid planets, and we may adopt a viscous model for the tidal dissipation (Eqs. 39, 40). Thermal atmospheric tides may also be present (e.g. Arras and Socrates 2010, 2009; Goodman 2009), but we did not take thermal tides into account, as gravitational tides are so strong for “Hot-Jupiters”, that they probably rule over all the remaining effects (see Sect. 3.3).

3.2.1. Rotational synchronization

The effect of gravitational tides over the obliquity is to straighten the spin axis (Eq. 45), so we will adopt $\varepsilon = 0^\circ$ for the obliquity. Assuming that the eccentricity and the semi-major axis of the planet are constant, we can derive from expression (39):

$$\frac{\omega}{n} = \frac{f_2(e)}{f_1(e)} + \left(\frac{\omega_0}{n} - \frac{f_2(e)}{f_1(e)} \right) \exp(-t/\tau_{eq}), \quad (93)$$

where $\tau_{eq}^{-1} = K f_1(e)/C$ is the characteristic time-scale for fully despinning the planet.

As for Mercury, the final equilibrium rotation driven by tides ($t \rightarrow +\infty$) is given by the equilibrium position $\omega_e/n = f_2(e)/f_1(e)$, which is different from synchronous rotation if the eccentricity is not zero (Fig. 4). Unlike Mercury, because “Hot-Jupiters” are assumed to be fluid, they should not present much irregularities in the internal structures. Therefore $(B - A)/C \approx 0$ and we do not expect

“Hot-Jupiters” to be captured in spin-orbit resonances. Indeed, determination of second-degree harmonics of Jupiter and Saturn’s gravity field from Pioneer and Voyager tracking data (Campbell and Anderson 1989) provided a crude estimate of the $(B - A)/C$ value lower than $\sim 10^{-5}$ for Saturn and $\sim 10^{-7}$ for Jupiter. The $(B - A)/C$ values for Jupiter and Saturn are more than one order of magnitude smaller than the Moon’s or Mercury’s value, leading to insignificant chances of capture. Furthermore, the detection of an equatorial asymmetry is questionable. If an equatorial bulge originates from local mass inhomogeneities driven by convection, it is probably not permanent and must have a more negligible effect if averaged spatially and temporally.

The time required for dampening the rotation of the planet depends on the dissipation factor $k_2 \Delta t$ (Eq. 43). Assuming that “Hot-Jupiters” are similar to the Solar System giant planets, we can adopt $k_2 = 0.4$, and a range for Q from 10^4 to 10^5 (Table 3). The Q -factor and the time lag Δt can be relied using expressions (22) and (34):

$$Q^{-1} \approx \sigma \Delta t. \quad (94)$$

Since we are using a viscous model, for which Δt is made constant, Q will be modified across the evolution as Q is inversely proportional to the tidal frequency σ . The Q -factor for the Solar System gaseous planets is measured for their present rotation states, which correspond to less than one day (Table 3). We may then assume that exoplanets should present identical Q values when they were rotating as rapidly as Jupiter, that is, $Q_0^{-1} = \omega_0 \Delta t$. For $Q_0 = 10^4$ and $\omega_0 = 2\pi/10$ h, we compute a constant $\Delta t \approx 0.57$ s.

We have plotted in Figure 12, all known exoplanets, taken from The Extrasolar Planets Encyclopedia (<http://exoplanet.eu/>), that could have been tidally evolved. We consider that exoplanets are fully evolved if their rotation rate, starting with an initial period of 10 h, is dampened to a value such that $|\omega/n - f_2(e)/f_1(e)| < 0.01$. The curves represent the planets that are tidally evolved in a given time interval ranging from 0.001 Gyr to 10 Gyr. Figure 12 allows us to check whether the planet should be fully evolved. For a Solar type star, we can expect that all exoplanets that are above the 1 Gyr curve have already reached the equilibrium rotation ω_e . On the other hand, exoplanets that are

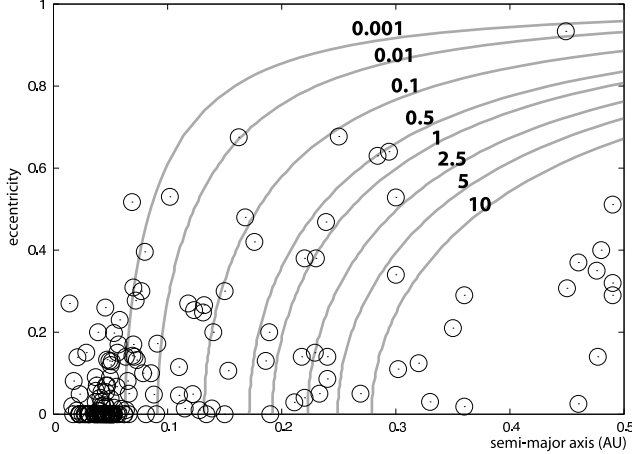


Fig. 12.— Tidally evolved exospins with $Q_0 = 10^4$ and initial rotation period $P_0 = 10$ h. The labeled curves denote (in Gyr) the time needed by the rotation to reach the equilibrium (time-scales are linearly proportional to Q_0). We assumed Jupiter’s geophysical parameters for all planets (Table 3) (updated from Laskar and Correia 2004).

below the 10 Gyr curve are probably not yet fully tidally evolved. As expected, all planets in circular orbits with $a < 0.05$ AU are tidally evolved. However, we are more interested on exoplanets further from the star with non zero eccentricity which are tidally evolved, since the rotation period is not synchronous, but given by expression (44). For instance, for the planet around HD 80606, the orbital period is 111.7 days, but since $e = 0.92$ we predict a rotation period of about 1.9 days.

3.2.2. Cassini states

Until now we have assumed that the final obliquity of the planet is zero degrees. However, Winn and Holman (2005) suggested that high obliquity values could be maintained if the planet has been trapped in a Cassini state resonance (Eq. 82) since the early despinning process. For small amplitude variations of the eccentricity and inclination, the equilibrium positions for the obliquity are given by expression (83). Unless $\alpha = |\nu_k|$, the state 1 is close to 0° , and state 3 is close to 180° . We thus focus only on state 2 that may maintain a significant obliquity.

To test the possibility of capture in the high oblique Cassini state 2, we can consider a simple scenario where a “Hot-Jupiter” forms at a large orbital distance (\sim several AUs) and migrates inward to the current position (~ 0.05 AU). Before the planet reaches typically ~ 0.5 AU, tidal effects do not affect the spin evolution, but the reduction in the semi-major axis increases the precession constant (Eq. 12), so that the precession frequency $\dot{\psi}$ may become resonant with some orbital frequencies ν_k (Eq. 80). The passage through resonance generally causes the obliquity to change (Ward 1975; Ward and Hamilton 2004; Hamilton and Ward 2004; Boué et al. 2009), rising the possibility that the obliquity has a somewhat arbitrary value

when the semi-major axis attains ~ 0.5 AU.

Tidal effects become efficient for $a < 0.5$ AU and drive the obliquity to an equilibrium value $\cos \varepsilon \approx 2n(1+6e^2)/\omega$ (Eq. 40). For initial fast rotation rates ($\omega \gg n$), the equilibrium obliquity tends to 90° . As the rotation rate is decreased by tides, the equilibrium obliquity is reduced to zero degrees (Eq. 45). It is then possible that the obliquity crosses several resonances (one for each frequency ν_k) in both ways (increasing and decreasing obliquity), and that a capture occurs. Inside the resonance island, the restoring torque causes the obliquity to librate with amplitude (Correia and Laskar 2003b):

$$\cos \varepsilon_2 \pm \Delta \cos \varepsilon_2 \approx -\frac{\nu_k}{\alpha} \pm 2\sqrt{\frac{\mathcal{J}_k}{\alpha} \sqrt{1 - \frac{\nu_k^2}{\alpha^2}}}. \quad (95)$$

Using a linear approximation of the tidal torque (Eq. 40) around the resonant obliquity ε_2 , the probability of capture in the Cassini state 2 can be estimated from the analytical approach for spin-orbit resonances (Eq. 73), with (Levrard et al. 2007a)

$$\frac{\Delta \omega}{\pi V n} = \left[\frac{(1 - 3 \cos^2 \varepsilon_2) \frac{\omega}{n} + 2 \cos \varepsilon_2}{\pi \sin^2 \varepsilon_2 (2 - \cos \varepsilon_2 \omega/n)} \right] \Delta \cos \varepsilon_2. \quad (96)$$

In Figure 13, we plotted the capture probabilities at 0.05, 0.1 and 0.5 AU as a function of the rotation period for different amplitudes (\mathcal{J}_k) and frequencies (ν_k) characteristic of the Solar System (Laskar and Robutel 1993). As a reasonable example, we choose $\nu_k = -10''/\text{yr}$, but the results are not affected by changes on this value. Assuming an initial rotation period of 12 h, the capture is possible and even unavoidable if $\mathcal{J}_k > 0.1''/\text{yr}$ at 0.5 AU. On the contrary, the chances of capture at 0.05 AU are negligible ($< 1\%$) because a decrease in the semi-major axis leads to an increase in the precession constant and reduces the width of the resonance (Eq. 95). Theoretical estimations can be compared with numerical simulations (Levrard et al. 2007a). To that purpose, the spin equations (Eqs. 79, 80) were integrated in the presence of tidal effects (Eqs. 39, 40) considering 1000 initial precession angles equally distributed over $0 - 2\pi$ for each initial obliquity. Statistics of capture were found to be in good agreement with previous theoretical estimates.

To test the influence of migration on the capture stability, additional numerical simulations were performed for various initial obliquities and secular perturbations over typically $\sim 5 \times 10^7$ yr. The migration process was simulated by an exponential decreasing of the semi-major axis towards 0.05 AU with a $10^5 - 10^7$ yr time scale. The obliquity librations were found to be significantly shorter than spin-down and migration time scales so that the spin trajectory follows an “adiabatic invariant” in the phase space. Nevertheless, expression (40) indicates that the tidal torque dramatically increases both with spin-down and inward migration processes ($d\varepsilon/dt \propto a^{-15/2} \omega^{-1}$). If the tidal torque exceeds the maximum possible restoring torque (Eq. 79), the resonant equilibrium is destroyed (the evolution is no longer

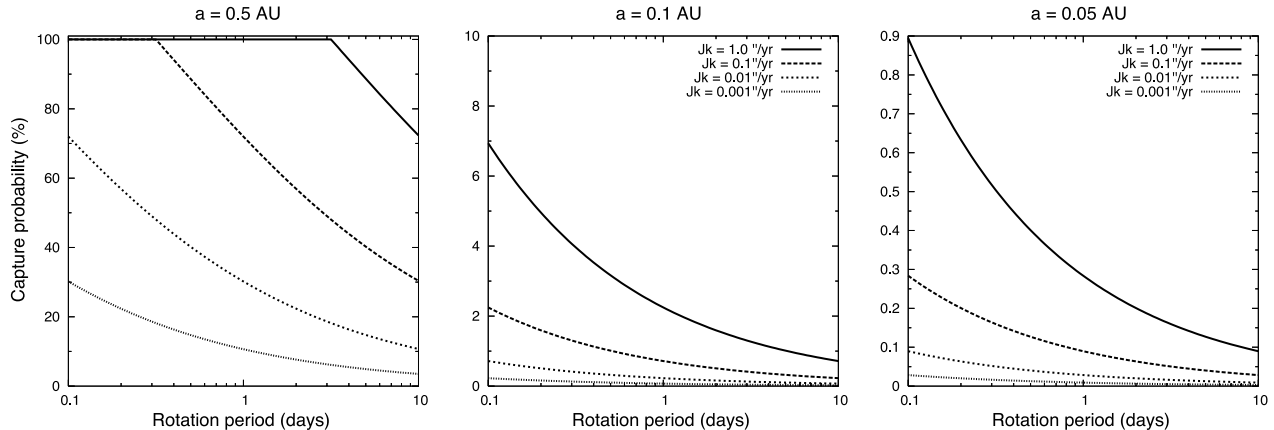


Fig. 13.— Obliquity capture probabilities in resonance under the effect of gravitational tides, as a function of the rotation period at a) 0.5 AU b) 0.1 AU c) 0.05 AU. \mathcal{J}_k is the amplitude of the secular orbital perturbations and $\nu_k = -10.0''/\text{yr}$ (Levrard et al. 2007a).

adiabatic). For a given semi-major axis, the stability condition requires then that the rotation rate must always be larger than a threshold value $\omega_{crit.}$, which is always verified if $\omega_{crit.} < f_2(e)/f_1(e)$. The stability condition can be simply written as (Levrard et al. 2007a)

$$\tan(\varepsilon) < \mathcal{J}_k \times \tau_{eq}, \quad (97)$$

where τ_{eq} is the time scale of tidal despinning (Eq. 93). It then follows that the final obliquity of the planet cannot be too large, otherwise the planet would quit the resonance. For instance, taking $\mathcal{J}_k = 1''/\text{yr}$ at 0.05 AU (the highest value in Fig. 13), we need an obliquity $\varepsilon < 21^\circ$. For the more realistic amplitude $\mathcal{J}_k = 0.1''/\text{yr}$, the resonant obliquity drops to $\varepsilon < 2^\circ$. Such a low resonant obliquity at 0.05 AU is highly unlikely, because, according to expression (83), the resonant state requires very high values of the orbital secular frequencies ($|\nu_k| > 7.2 \times 10^6''/\text{yr}$). At 0.5 and 0.1 AU, critical obliquity values are respectively 83° and 41° and require more reasonable orbital secular frequencies so that a stable capture is possible. In numerical simulation, the stability criteria for the final obliquity (Eq. 97) is empirically retrieved with an excellent agreement (Levrard et al. 2007a). When the obliquity leaves the resonance, the obliquity ultimately rapidly switches to the resonant stable Cassini state 1, which tends to 0° (Eq. 83). We then conclude that locking a “Hot-Jupiter” in an oblique Cassini state seems to be a very unlikely scenario.

3.2.3. Energy balance

Tidal energy is dissipated in the planet at the expense of the rotational and orbital energy so that $\dot{E} = -C\omega\dot{\omega} - \dot{a}(Gm_*m)/(2a^2)$. Replacing the equilibrium rotation given by equation (44) in expression (46) we obtain for the tidal energy:

$$\dot{E} = Kn^2 \left[f_3(e) - \frac{f_2^2(e)}{f_1(e)} \frac{2x^2}{1+x^2} \right], \quad (98)$$

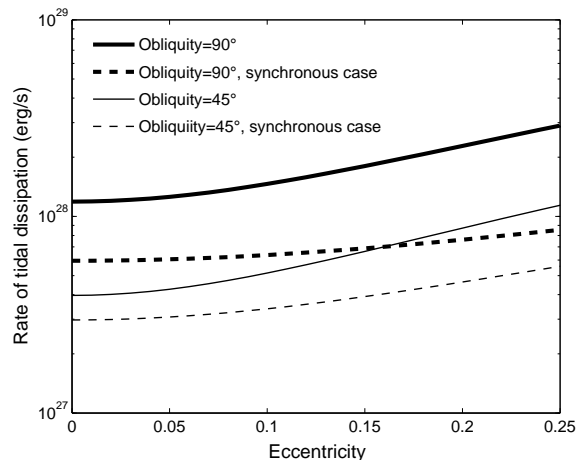


Fig. 14.— Rate of tidal dissipation within HD 209458 b as a function of the eccentricity for 45° (solid thin line) and 90° (solid thick line) obliquity. The synchronous case is plotted with dashed lines for comparison. The dissipation factor Q_0/k_2 is set to 10^6 (Levrard et al. 2007a).

or, at second order in eccentricity,

$$\dot{E} = \frac{Kn^2}{1 + \cos^2 \varepsilon} [\sin^2 \varepsilon + e^2 (7 + 16 \sin^2 \varepsilon)], \quad (99)$$

which is always larger than in the synchronous case (e.g. Wisdom 2004). In Figure 14 the rate of tidal heating within a non-synchronous and synchronous planet as a function of the eccentricity ($0 < e < 0.25$) is compared for two different obliquities (Levrard et al. 2007a). The ratio between the tidal heating in the two situations is an increasing function of both eccentricity and obliquity. For $e \approx 0$, as observed for “Hot-Jupiters”, the ratio may reach ~ 1.3 and 2.0 at respectively 45° and 90° obliquity, not being significantly modified at larger eccentricity.

We then conclude that planets in eccentric orbits and/or with high obliquity dissipate more energy than planets in synchronous circular orbits. This may explain why some

planets appear to be more inflated than initially expected (e.g. Knutson et al. 2007). A correct tidal energy balance must then take into account the present spin and eccentricity of the orbit.

3.2.4. Orbital circularization

In Sect. 2.2.4 we saw that under tidal friction the spin of the planet attains an equilibrium position faster than the orbit. As a consequence, we can use the expression of the equilibrium rotation rate (Eq. 44) in the semi-major axis and eccentricity variations and find simplified expressions (Eqs. 51 and 52). Combining the two equations we get

$$\frac{da}{a} = \frac{2e de}{(1 - e^2)}, \quad (100)$$

whose solution is given by

$$a = a_f(1 - e^2)^{-1}. \quad (101)$$

Replacing the above relation in expression (52) we find a differential equation that rules the eccentricity evolution:

$$\dot{e} = -K_0 f_6(e)(1 - e^2)^9 e, \quad (102)$$

where K_0 is a constant parameter:

$$K_0 = \Delta t \frac{21k_2 G m_*^2 R^5}{2\mu a_f^8}. \quad (103)$$

The solution of the above equation is given by

$$F(e) = F(e_0)e^{-K_0 t}, \quad (104)$$

where $F(e)$ is an implicit function of e , which converges to zero as $t \rightarrow +\infty$. For small eccentricities, we can neglect terms in e^4 and $F(e) = e|7 - 9e^2|^{-1/2}$. The characteristic time-scale for fully dampening the eccentricity of the orbit is then $\tau_{orb} \sim 1/K_0$, and the ratio between the spin and orbital time-scales

$$\frac{\tau_{eq}}{\tau_{orb}} \sim \left(\frac{R}{a_f}\right)^2. \quad (105)$$

Since $a_f = a(1 - e^2)$, for initial very eccentric orbits the two time-scales become comparable.

We have plotted in Figure 15, all known exoplanets, taken from The Extrasolar Planets Encyclopedia (<http://exoplanet.eu/>), whose orbits could have been tidally evolved. We consider that they are fully evolved if the eccentricity is dampened to a value $e < 0.01$. The curves represent the time needed to damp the eccentricity starting with the present orbital parameters, for time intervals ranging from 0.001 Gyr to 100 Gyr. Figure 15 allows us to simultaneously check whether the planet is tidally evolved, and the time needed to fully damp the present eccentricity. All planets in eccentric orbits experience stronger tidal effects because the planet is close to the star at the periape. As a consequence, tidal friction

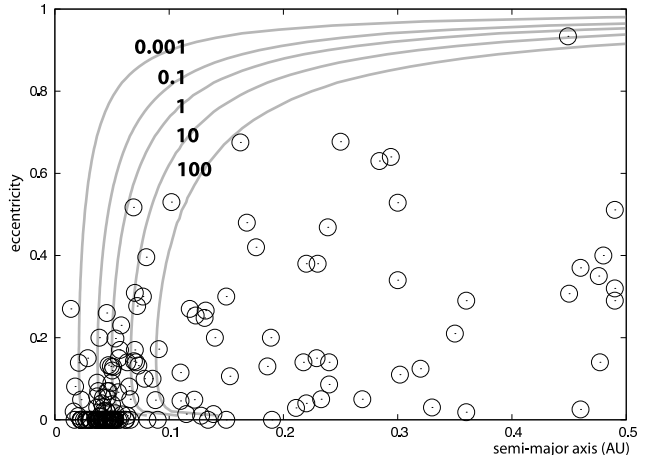


Fig. 15.— Tidally evolved orbits of exoplanets with $Q_0 = 10^4$. The labeled curves denote (in Gyr) the time needed to circularize the orbits of the planets ($e < 0.01$) (time-scales are linearly proportional to Q_0). We assumed Jupiter’s geophysical parameters for all planets (Table 3).

can, under certain conditions, be an important mechanism for the formation of “Hot-Jupiters” (see Sect. 3.2.5).

According to Figure 15, a significant fraction of exoplanets that are close to the host star ($a < 0.1$ AU) still present eccentricities up to 0.4, although tidal effects should have already damped the eccentricity to zero. Observational errors and/or weaker tidal dissipation ($Q_0 \gg 10^4$) can be a possible explanation, but they will hardly justify all the observed situations. A more plausible explanation is that the eccentricity of the exoplanet is being excited by gravitational perturbations from an outer planetary companion (Sect. 2.5). Indeed, the eccentricity of a inner short-period planet can be excited as long as its (non-resonant) outer companion’s eccentricity is non-zero. Mardling (2007) has shown that the eccentricity of the outer planet will decay on a time-scale which depends on the structure of the inner planet, and that the eccentricities of both planets are damped at the same rate, controlled by the outer planet (Fig. 16). The mechanism is so efficient that the outer planet may be an Earth-mass planet in the “habitable zones” of some stars. As a consequence, the evolution time-scale for both eccentricities can attain the Gyr instead of Myr, which could explain the current observations of non-zero eccentricity for some “Hot-Jupiters”.

3.2.5. Kozai migration

In current theories of planetary formation, the region within 0.1 AU of a protostar is too hot and rarefied for a Jupiter-mass planet to form, so “Hot-Jupiters” likely form further away and then migrate inward. A significant fraction of “Hot-Jupiters” has been found in systems of binary stars (e.g. Eggenberger et al. 2004), suggesting that the stellar companion may play an important role in the shrinkage of the planetary orbits. In addition, close binary star systems (separation comparable to the stellar radius) are also often

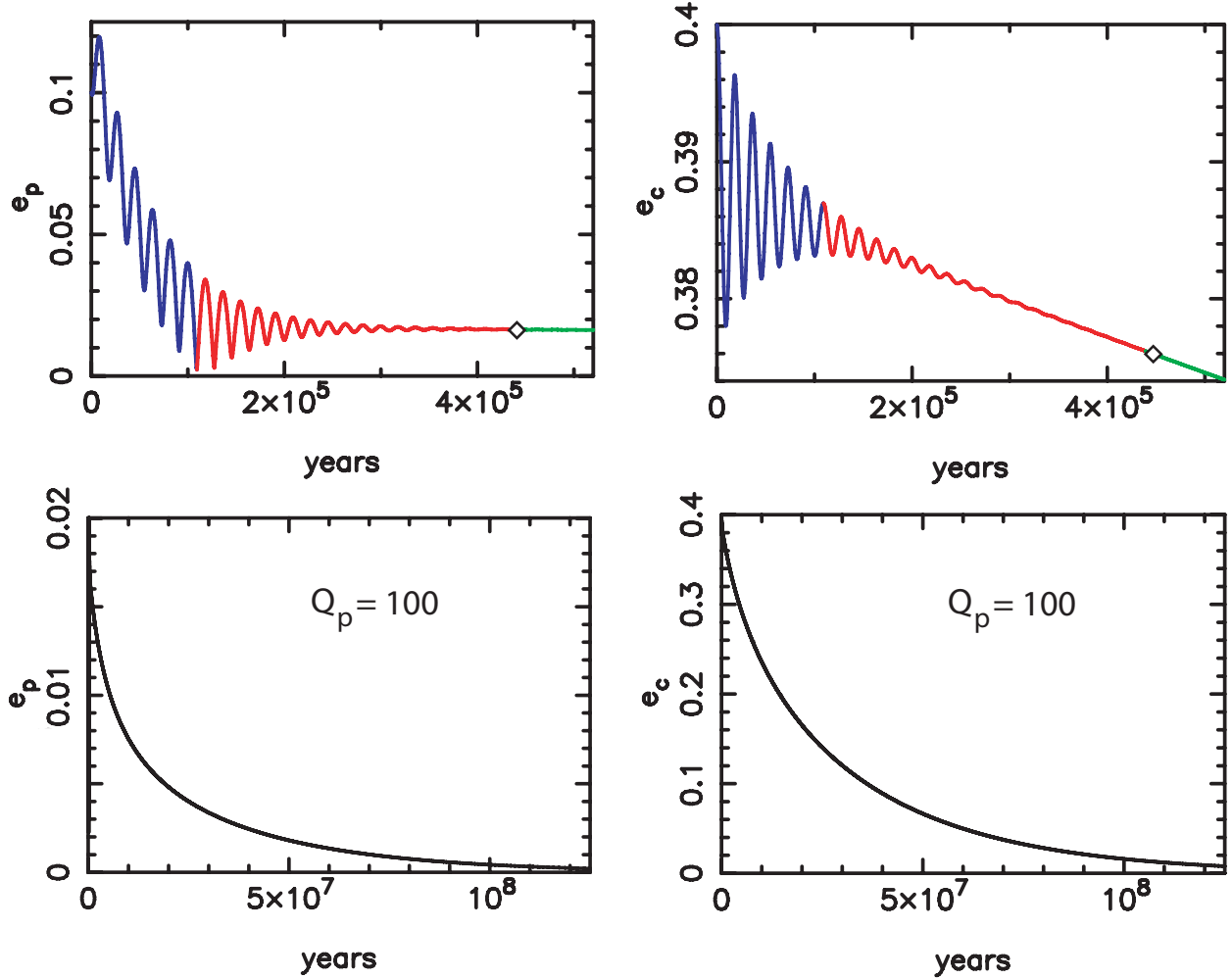


Fig. 16.— Tidal evolution of the eccentricities of planet HD209458 b (e_p) perturbed by a $0.1M_{\text{Jup}}$ companion at 0.4 AU (e_c). The dissipation factor $Q_p = 100$ of the observed planet is set artificially low in order to illustrate the damping process (time-scales are linearly proportional to Q_p). Top figures show the first stages of the evolution. The change in grayscale shows the transition of the eccentricity from the circulation phase to the libration phase. The diamond represents the moment where the eccentricity librations are damped. Bottom figures show the final evolution of the eccentricities. The presence of a companion result that e_p decays at the same rate of e_c , while the dissipation rate for e_c is controlled by Q_p and not by Q_c (Mardling 2007).

accompanied by a third star. For instance, Tokovinin et al. (2006) found that 96% of a sample of spectroscopic binaries with periods less than 3 days has a tertiary component. Indeed, in some circumstances the distant companion enhances tidal interactions in the inner binary, causing the binary orbital period to shrink to the currently observed values.

Three-body systems can be stable for long-time scales provided that the system is hierarchical, that is, if the system is formed by an inner binary (star and planet) in a nearly Keplerian orbit with a semi-major axis a , and a outer star also in a nearly Keplerian orbit about the center of mass of the inner system with semi-major $a' \gg a$. An additional requirement is that the eccentricity e' of the outer orbit is not too large, in order to prevent close encounters with the inner system. In this situation, perturbations on the inner planetary orbit are weak, but can have important long-term

effects (Chapter 10: *Non-Keplerian Dynamics*).

The most striking effect is known as the Lidov-Kozai mechanism (Kozai 1962; Lidov 1962), which allows the inner orbit to periodically exchange eccentricity with inclination. Even at large distances ($a' > 1000$ AU), the outer star can significantly perturb the planetary orbit as long as the two orbital planes are initially inclined to each other more than $I > 39.2^\circ$ (that is, for $\cos I < (3/5)^{1/2}$). When $I < 39.2^\circ$ there is little variation in the planet's inclination and eccentricity. Secular effects of the Lidov-Kozai type can then produce large cyclic variations in the planet's eccentricity e as a result of angular momentum exchange with the companion orbit. Since the z -component of the planet's angular momentum must be conserved and a is not modified by the secular perturbations, the Kozai integral

$$L_K = (1 - e^2)^{1/2} \cos I \quad (106)$$

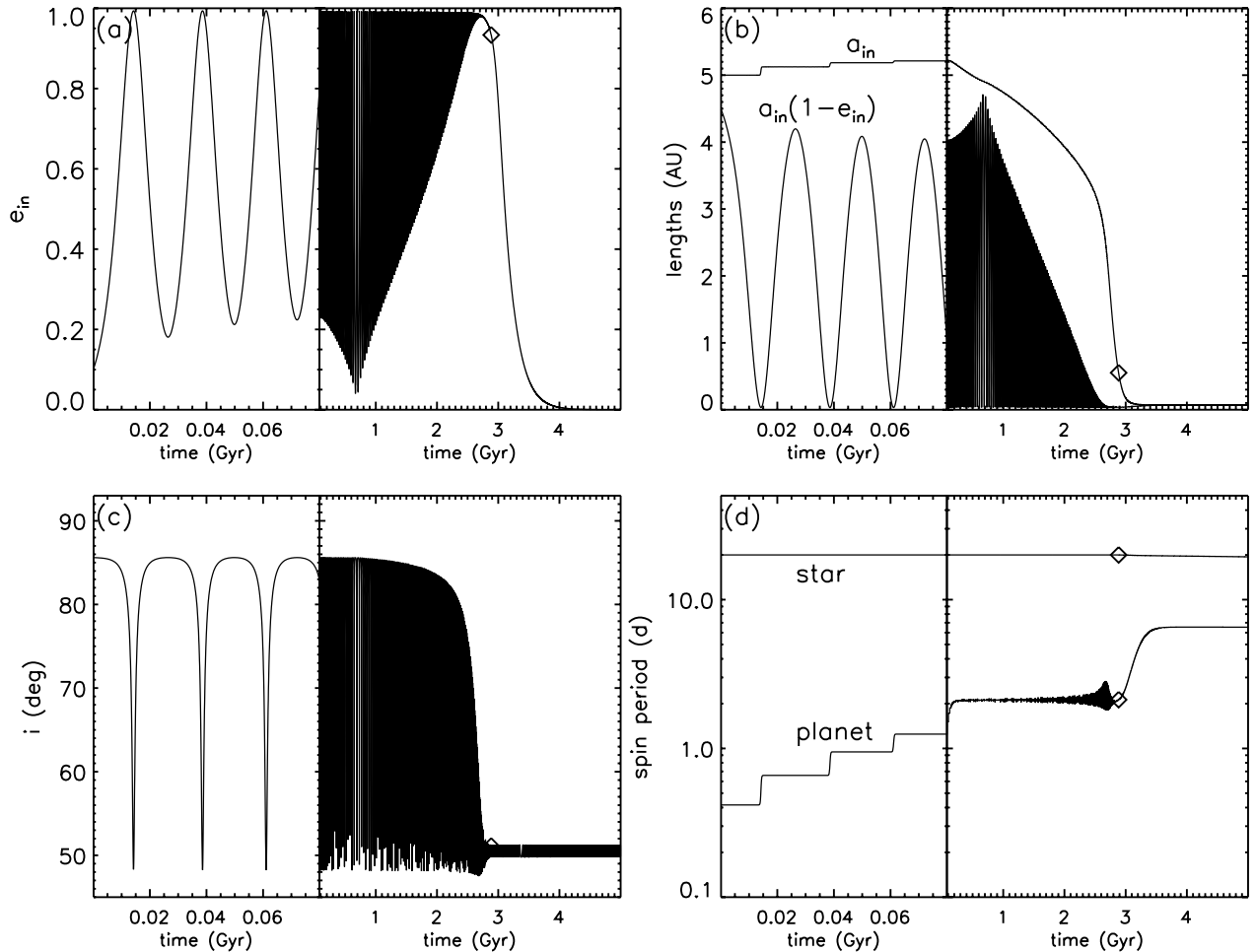


Fig. 17.— Possible evolution of the planet HD 80606 b initially in an orbit with $a = 5$ AU, $e = 0.1$, and $I = 85.6^\circ$. The stellar companion is supposed to be a Sun-like star at $a' = 1000$ AU, and $e' = 0.5$. The diamonds mark the current position of HD 80606 b along this possible evolution (Wu and Murray 2003; Fabrycky and Tremaine 2007).

is conserved during the oscillations (Lidov and Ziglin 1976). Maxima in e occur with minima in I , and vice versa. If the inner orbit is initially circular, the maximum eccentricity achieved in a Kozai cycle is $e_{max} = (1 - (5/3) \cos^2 I)^{1/2}$ and the oscillation period of a cycle is approximately P'^2/P (Kiseleva et al. 1998). The maximum eccentricity of the inner orbit in the Kozai cycle will remain fixed for different masses and distances of the outer star, but the period of the Kozai cycle will grow with a'^3 . Kozai cycles persist as long as the perturbation from the outer star is the dominant cause of periape precession in the planetary orbit. However, small additional sources of periape precession such as the quadrupole moments, additional companions, general relativity or even tides can compensate the Kozai precession and suppress the eccentricity/inclination oscillations (e.g. Migaszewski and Goździewski 2009).

Because the Lidov-Kozai mechanism is able to induce large eccentricity excitations, a planet in an initial almost circular orbit (for instance a Jupiter-like planet at 5 AU around a Sun-like star) can experiment close approaches to the host star at the periape when the eccentricity increases

to very high values. As a consequence, tidal effects increase several orders of magnitude and according to expression (51) the semi-major axis of the orbit will decrease and the planet migrate inward. At some point of the evolution, the periape precession will be dominated by other effects and the eccentricity oscillations suppressed. From that moment on, the eccentricity is damped according to expression (52) and the final semi-major axis given by $a_f = a(1 - e^2)$. Ford and Rasio (2006) have derived that tidal evolution of high eccentric orbits would end at a semi major axis a_f equal to about twice the Roche limit R_L . Indeed, at the closest periape distance, attained for $e \approx 1$, we will have $a(1 - e) = R_L$, and thus $a_f = (1 + e)R_L \approx 2R_L$.

In Figure 17 we plot an example of combined Kozai-tidal migration of the planet HD 80606 b. The planet is initially set in an orbit with $a = 5$ AU, $e = 0.1$, and $I = 85.6^\circ$. The stellar companion is supposed to be a Sun-like star at $a' = 1000$ AU, and $e' = 0.5$ (Wu and Murray 2003; Fabrycky and Tremaine 2007). Prominent eccentricity oscillations are seen from the very beginning and the energy in the planet's spin is transferred to the orbit increasing the

semi-major axis for the first 0.1 Gyr (Eq. 39). As the equilibrium rotation is achieved (Eq. 44) the orbital evolution is essentially controlled by equations (51) and (52), whose contributions are enhanced when the eccentricity reaches high values. The semi-major axis evolution is executed by apparent “discontinuous” transitions precisely because the tidal dissipation is only efficient during periods of high eccentricity. As dissipation shrinks the semi-major axis, periape precession becomes gradually dominated by relativity rather than by the third body, and the periape starts circulating as the eccentricity passes close to 0 at 0.7 Gyr. Tidal evolution stops when the orbit is completely circularized. The present semi-major axis and eccentricity of planet HD 80606 b are $a = 0.45$ AU and $e = 0.92$, respectively, meaning that the tidal evolution on HD 80606 b is still under way (Fig. 15). The final semi-major axis is estimated to about $a_f = 0.07$ AU, which corresponds to a regular “Hot-Jupiter”.

3.3. “Super-Earths”

After a significant number of discoveries of gaseous giant exoplanets, a new barrier has been passed with the detections of several exoplanets in the Neptune and even Earth-mass (M_\oplus) regime: $2 - 12 M_\oplus$ (Rivera et al. 2005; Lovis et al. 2006; Udry et al. 2007; Bonfils et al. 2007), that are commonly designated by “Super-Earths”. If the commonly accepted core-accretion model can account for the formation of “Super-Earths”, resulting in a mainly icy/rocky composition, the fraction of the residual He- H_2 atmospheric envelope accreted during the planet migration is not tightly constrained for planets more massive than the Earth (e.g. Alibert et al. 2006). A minimum mass of below $10 M_\oplus$ is usually considered to be the boundary between terrestrial and giant planets, but Rafikov (2006) found that planets more massive than $6 M_\oplus$ could have retained more than $1 M_\oplus$ of the He- H_2 gaseous envelope. For comparison, masses of Earth’s and Venus’ atmosphere are respectively $\sim 10^{-6}$ and 10^{-4} times the planet’s mass. Despite significant uncertainties, the discoveries of “Super-Earths” provide an opportunity to test some properties that could be similar to those of the more familiar terrestrial planets of the Solar System.

Because some of the “Super-Earths” are potentially in the “habitable zone” (Udry et al. 2007; Selsis et al. 2007), the present spin state is an important factor to constrain the climates. As for Venus, thermal atmospheric tides may have a profound influence on the spin of “Super-Earths”. However, the small eccentricity approximation done for Venus (Eq. 87) may no longer be adequate for “Super-Earths”, which exhibit a wide range of eccentricities, orbital distances, or central star types. Although our knowledge of “Super-Earths” is restricted to their orbital parameters and minimum masses, we can attempt to place new constraints on the surface rotation rate, assuming that “Super-Earths” have a dense atmosphere.

As for Venus, the combined effect of tides is to set the

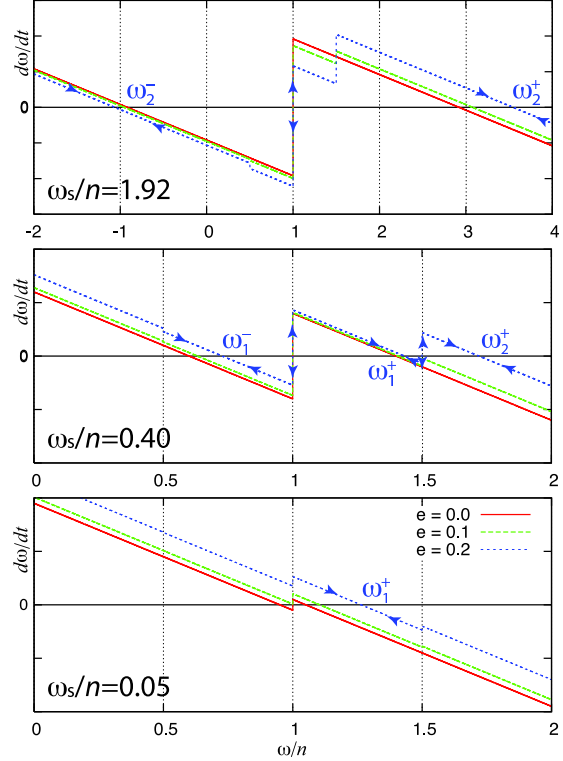


Fig. 18.— Evolution of $\dot{\omega}$ (Eq. 107) with ω/n for different atmospheric strengths ($\omega_s/n = 1.92, 0.40, 0.05$) and eccentricities ($e = 0.0, 0.1, 0.2$). The top picture with $e = 0$ is the same as Figure 8 for Venus. The equilibrium rotation rates are given by $\dot{\omega} = 0$ and the arrows indicate whether the equilibrium position is stable or unstable. For $\omega_s/n > 1$, we have two equilibrium possibilities, ω_2^\pm , one of which corresponds to a retrograde rotation (as for Venus). For $\omega_s/n < 1$, retrograde states are not possible, but we can still observe final rotation rates $\omega^- < n$. For eccentric orbits, because of the harmonics in $\sigma = 2\omega - n$ and $\sigma = 2\omega - 3n$, we may have at most four different final possibilities (Eq. 110). When ω_s/n becomes extremely small, which is the case for the present observed exoplanets with some eccentricity (Table 4), a single final equilibrium is possible for ω_1^+ (Correia et al. 2008).

final obliquity at 0° or 180° (Correia et al. 2003). Adopting a viscous dissipation model for tidal effects (Eq. 37) and the “heating at the ground” model (Dobrovolskis and Ingersoll 1980) for surface pressure variations (Eq. 68), the average evolution of the rotation rate is then obtained by adding the effects of both tidal torques acting on the planet. From expressions (23) and (60) we get for $\varepsilon = 0^\circ$ and to the second order in the eccentricity:

$$\frac{\dot{\omega}}{\tau_{eq}} = \omega - (1 + 6e^2)n - \omega_s \left[\left(1 - \frac{21}{2}e^2\right) \text{sign}(\omega - n) - e^2 \text{sign}(2\omega - n) + 9e^2 \text{sign}(2\omega - 3n) \right], \quad (107)$$

where

$$\omega_s = \frac{F_s}{16H_0k_2} \frac{K_a \Delta t_a}{K_g \Delta t_g} \propto \frac{L_\star}{m_\star} \frac{R}{m} a. \quad (108)$$

When $e = 0$, we saw in the case of Venus that final positions of the rotation rate at zero obliquity are given by

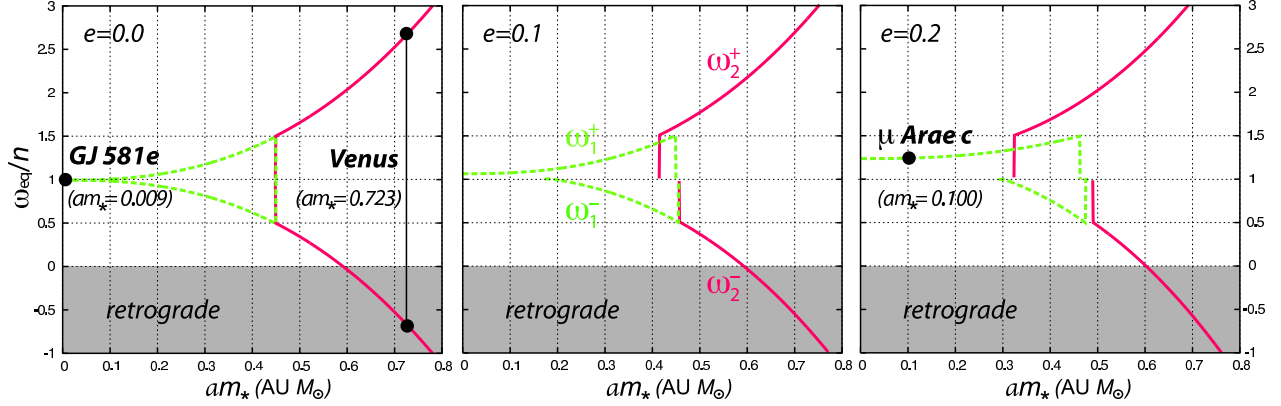


Fig. 19.— Equilibrium positions of the rotation rate for “Super-Earths” as a function of the product am_* for three different values of the eccentricity ($e = 0.0, 0.1, 0.2$). Each curve corresponds to a different final state (dotted lines for ω_1^\pm and solid lines for ω_2^\pm). For $e \approx 0$ (case of Venus), we always count two final states that are symmetrical about n . For small values of am_* , the two equilibrium possibilities are so close to n that the most likely scenario for the planet is to be captured in the synchronous resonance (case of GJ 581 e). As we increase the eccentricity, we can count at most three final equilibrium rotations, depending on the value of ω_s/n (computed from Eq. 114). When $e \approx 0.2$, only one equilibrium state exists for $am_* < 0.3$, resulting from $\omega_s/n < 6e^2(1 + e^2/2)$. This is the present situation of μ Arae c and most of the “Super-Earths” listed in Table 4 (Correia et al. 2008).

(Eq. 90):

$$|\omega - n| = \omega_s, \quad (109)$$

i.e., there are two final possibilities for the equilibrium rotation of the planet, given by $\omega^\pm = n \pm \omega_s$. When $e \neq 0$, the above expression (109) is no longer valid and additional equilibrium positions for the rotation rate may occur. For moderate values of the eccentricity, from expression (107) we have that the effect of the eccentricity is eventually to split each previous equilibrium rotation rate into two new equilibrium values. Thus, four final equilibrium positions for the rotation rate are possible (eight if we consider the case $\varepsilon = 180^\circ$), obtained with $\dot{\omega} = 0$ (Fig. 18):

$$\omega_{1,2}^\pm = n \pm \omega_s + e^2 \delta_{1,2}^\pm, \quad (110)$$

with

$$\delta_1^- = 6n + \frac{1}{2}\omega_s, \quad \delta_1^+ = 6n - \frac{41}{2}\omega_s, \quad (111)$$

and

$$\delta_2^- = 6n + \frac{5}{2}\omega_s, \quad \delta_2^+ = 6n - \frac{5}{2}\omega_s. \quad (112)$$

Because the set of $\omega_{1,2}^\pm$ values must verify the additional condition

$$\omega_2^- < n/2 < \omega_1^- < n < \omega_1^+ < 3n/2 < \omega_2^+, \quad (113)$$

the four equilibrium rotation states cannot, in general, exist simultaneously, depending on the values of ω_s and e . In particular, the final states ω_1^- and ω_1^+ can never coexist with ω_2^- . At most three different equilibrium states are therefore possible, obtained when ω_s/n is close to $1/2$, or more precisely, when $1/2 - 19e^2/4 < \omega_s/n < 1/2 + 17e^2/4$. Conversely, we find that one single final state $\omega_1^+ = (1 + 6e^2)n + (1 - 41e^2/2)\omega_s$ exists when $\omega_s/n < 6e^2(1 + e^2/2)$.

The Earth and Venus are the only planets that can be included in the category of “Super-Earths” for which the atmosphere and spin are known. Only Venus is tidally evolved and therefore suitable for applying the above expressions for tidal equilibrium. We can nevertheless investigate the final equilibrium rotation states of the already detected “Super-Earths”. For that purpose, we considered only exoplanets with masses smaller than $12 M_\oplus$ that we classified as rocky planets with a dense atmosphere, although we stress that this mass boundary is quite arbitrarily.

Using the empirical mass-luminosity relation $L_* \propto M_*^4$ (e.g. Cester et al. 1983) and the mass-radius relationship for terrestrial planets $R \propto m^{0.274}$ (Sotin et al. 2007), expression (108) can be written as:

$$\omega_s/n = \kappa (am_*)^{2.5} m^{-0.726}, \quad (114)$$

where κ is a proportionality coefficient that contains all the constant parameters, but also the parameters that we are unable to constrain such as H_0 , k_2 , Δt_g or Δt_a . In this context, as a first order approximation we consider that for all “Super-Earths” the parameter κ has the same value as for Venus. Assuming that the rotation of Venus is presently stabilized in the ω^- final state, that is, $2\pi/\omega^- = -243$ days (Carpenter 1970), we compute $2\pi/\omega_s = 116.7$ days. Replacing the present rotation in expression (114), we find for Venus that $\kappa = 3.723 M_\oplus^{0.726} M_\odot^{-2.5} \text{AU}^{-2.5}$. We can then estimate the ratio ω_s/n for all considered “Super-Earths” in order to derive their respective equilibrium rotation rates (Table 4).

The number and values of the allowed equilibrium rotation states are plotted as a function of aM_* for different eccentricities in Figure 19. All eccentric planets have a ratio ω_s/n that is lower than 6×10^{-3} (Table 4), which verifies the condition $\omega_s/n < 6e^2(1 + e^2/2)$. As a consequence, only one single final state exists $\omega_1^+/n \approx (1 + 6e^2)$, cor-

TABLE 4

CHARACTERISTICS AND EQUILIBRIUM ROTATIONS OF SOME “SUPER-EARTHS” WITH MASSES LOWER THAN $12 M_{\oplus}$

Name	m_{\star} [M_{\odot}]	Age [Gyr]	τ_{eq} [Gyr]	$m \sin i$ [M_{\oplus}]	a [AU]	e	ω_s/n	$2\pi/n$ [day]	$2\pi/\omega_2^-$ [day]	$2\pi/\omega_1^-$ [day]	$2\pi/\omega_1^+$ [day]	$2\pi/\omega_2^+$ [day]
Venus	1.00	4.5	2.3	0.82	0.723	0.007	1.92	224.7	-243.0			76.8
Earth*	1.00	4.5	16	1.00	1.000	0.017	3.75	365.3	-132.9			77.1
¹ GJ 581 e	0.31	7-11	10^{-7}	1.94	0.03	0	10^{-5}	3.4087		3.4088	3.4087	
² HD 40307 b	0.77	—	10^{-7}	4.2	0.047	0	0.0003	4.2413		4.2427	4.240	
¹ GJ 581 c	0.31	7-11	10^{-5}	5.36	0.07	0.17	10^{-4}	12.14			10.6335	
³ GJ 876 d	0.32	9.9	10^{-8}	6.3	0.021	0.14	10^{-6}	1.9649			1.7822	
² HD 40307 c	0.77	—	10^{-5}	6.9	0.081	0	0.0009	9.5956		9.6042	9.5871	
¹ GJ 581 d	0.31	7-11	0.02	7.09	0.22	0.38	0.0011	67.6918			47.8226	
⁴ HD 181433 b	0.78	—	10^{-5}	7.5	0.08	0.396	0.0008	9.3579			6.535	
⁵ GJ 176 b	0.5	—	10^{-5}	8.4	0.066	0	0.0002	8.7583		8.7596	8.7568	
² HD 40307 d	0.77	—	10^{-4}	9.2	0.134	0	0.0025	20.4175		20.4696	20.3656	
⁶ HD 7924 b	0.83	—	10^{-6}	9.26	0.057	0.17	0.0004	5.4493			4.7688	
⁷ HD 69830 b	0.86	4-10	10^{-5}	10.2	0.079	0.10	0.0008	8.6625			8.1995	
⁸ μ Arae c	1.1	6.41	10^{-5}	10.6	0.091	0.172	0.0021	9.5505			8.13313	
⁹ 55 Cnc e	1.03	5.5	10^{-7}	10.8	0.038	0.07	0.0002	2.6659			2.592	
¹⁰ GJ 674 b	0.35	0.1-1	10^{-7}	11.09	0.039	0.2	10^{-5}	4.7549			4.0138	
⁷ HD 69830 c	0.86	4-10	10^{-3}	11.8	0.186	0.13	0.0064	31.5943			28.8691	

(*) Moon tidal effects were not included. τ_{eq} was computed with $k_2 = 1/3$ and $\Delta t_g = 640$ s (Earth’s values). References: [1] Mayor et al. (2009a); [2] Mayor et al. (2009b); [3] Correia et al. (2010); [4] Bouchy et al. (2009); [5] Forveille et al. (2009); [6] Howard et al. (2009); [7] Lovis et al. (2006); [8] Pepe et al. (2007); [9] Fischer et al. (2008); [10] Bonfils et al. (2007).

responding to the equilibrium rotation resulting from gravitational tides (Eq. 44). The main reason is that the effect of atmospheric tides is clearly disfavored relative to the effect of gravitational tides on “Super-Earths” discovered orbiting M-dwarf stars: the short orbital periods strengthens the effect of gravitational tides, which are proportional to $1/a^6$, while the effect of thermal tides varies as $1/a^5$. Moreover, the small mass of the central star also strongly affects the luminosity received by the planet and hence the size of the atmospheric bulge driven by thermal contrasts.

For the planets with nearly zero eccentricity (GJ 581 e, HD 40307 b, c, d, and GJ 176 b), two equilibrium rotation states ω_1^{\pm} are possible. However, the two final states ω_1^{\pm} are so close to the mean motion n , that the quadrupole moment of inertia $(B - A)/C$ will probably capture the rotation of the planet in the synchronous resonance. We then conclude that “Super-Earths” orbiting close to their host stars (in particular M-dwarfs), will be dominated by gravitational tides and present a final equilibrium rotation rate given by $\omega_e/n \approx f_2(e)/f_1(e)$ (Fig. 4), or present spin-orbit resonances like Mercury.

4. FUTURE PROSPECTS

The classical theory of tides initiated by Darwin (1880, 1908) is sufficient to understand the main effects of tidal friction upon planetary evolution. However, the exact mechanism on how tidal energy is dissipated within the

internal layers of the planet remains a challenge for planetary scientists. Kaula (1964) derived a generalization of Darwin’s work, with consideration of higher order tides and without the adoption of any dissipation model. The tidal potential is described using infinite series in eccentricity and inclination, which is not practical and can only be correctly handled by computers. Ever since many efforts have been done in order to either simplify the tidal equations, or to correctly model the tidal dissipation (for a review see Ferraz-Mello et al. 2008; Efroimsky and Williams 2009).

Many Solar System phenomena have been successfully explained using the existent tidal models, so we expect that they are suitable to describe the tidal evolution of exoplanets. Nevertheless, many exoplanets are totally different from the Solar System cases, and we cannot exclude to observe some unexpected behaviors. For instance, it is likely that dissipation within “Hot-Jupiters” is closer to dissipation within stars (e.g. Zahn 1975), while dissipation within “Super-Earths” is closer to dissipation observed for rocky planets (e.g. Henning et al. 2009). It is then necessary to continue improving tidal models in order to get a more realistic description for each planetary system. In particular, a correct description of the tidal dissipation and on how it evolves with the tidal frequency is critical for the evolution time-scale.

The orbital architecture of exoplanetary systems is relatively well determined from the present observational techniques. However, the spins of the exoplanets are not easy to

measure, as the light curve coming from the planet is always dimmed by the star light. The continuous improvements that have been made in photometry and spectrography let us believe that the determination of exoplanets' spins can be a true possibility in the near future. In particular, infrared spectrographs are being developed, which will allow to acquire spectra of the planets if we manage to subtract the stellar contribution (e.g. Barnes et al. 2010).

Some additional methods for detecting the rotation and/or the obliquity of exoplanets have also been tested and suggested so far. For instance, indirect sensing of the planetary gravitational quadrupole and shape, which is linked to both spin rate and obliquity (e.g. Seager and Hui 2002; Ragozzine and Wolf 2009), or transient heating of one face of the planet, which then spins into and out of view, as it has been attempted for the system HD 80606 (Laughlin et al. 2009). The effect of planetary rotation on the transit spectrum of a giant exoplanet is another possibility. During ingress and egress, absorption features arising from the planet's atmosphere are Doppler shifted by of order the planet's rotational velocity ($\sim 1\text{-}2\text{ km s}^{-1}$) relative to where they would be if the planet were not rotating (e.g. Spiegel et al. 2007). Finally, for planets whose light is spatially separated from the star, variations may be discernible in the light curve obtained by low-precision photometry due to meteorological variability, composition of the surface, or spots (e.g. Ford et al. 2001).

Although the spin states of exoplanets cannot be measured, for exoplanets that are tidally evolved we can still try to make predictions for the rotation rates. When the eccentricity is large, the rotation of many of the observed exoplanets can still be tidally evolved even if the planets are not very close to their central stars (Fig. 12). For tidally evolved "Hot-Jupiters", we can conjecture that the rotation periods are the limit values $P_{orb} \times f_1(e)/f_2(e)$ (Fig. 4). It becomes a new challenge for the observers to be able to confirm these predictions.

Thermal atmospheric tides may very well destabilize the tidal equilibrium from gravitational tides and create additional possible stable limit values, with the possibility of retrograde rotations, as for planet Venus (Fig. 8). Thermal tides should be particularly important for "Super-Earths", which are expected to have a distinct rocky body surrounded by a dense atmosphere. In a paradoxical way, the final rotation rate of "Super-Earths" are the most difficult to predict, as the equilibrium configurations depend on the composition of the atmospheres. Thermal tides are nevertheless more relevant for exoplanets that orbit Sun-like stars at not very close distances, like Venus (Fig. 19).

We also assumed that the final obliquity of exoplanets is either 0° or 180° , as the two values represent the final outcome of tidal evolution. However, each planetary system has its own architecture, and planetary perturbations on the spin can lead to resonant capture in a high oblique Cassini states or even to chaotic motion. Thus, the final spin evolution of a planet cannot be dissociated from its environment, and a more realistic description of exoplanets rotation can

only be achieved with the full knowledge of the system orbital dynamics.

Acknowledgments. We thank to an anonymous referee for valuable suggestions, who helped to improve this work. We acknowledge support from the Fundação para a Ciência e a Tecnologia (Portugal) and PNP-CNRS (France).

REFERENCES

- Abramowitz, M., Stegun, I. A., 1972. Handbook of Mathematical Functions. Dover, New York.
- Agnor, C. B., Canup, R. M., Levison, H. F., Nov. 1999. On the Character and Consequences of Large Impacts in the Late Stage of Terrestrial Planet Formation. *Icarus* 142, 219–237.
- Alibert, Y., Baraffe, I., Benz, W., Chabrier, G., Mordasini, C., Lovis, C., Mayor, M., Pepe, F., Bouchy, F., Queloz, D., Udry, S., Aug. 2006. Formation and structure of the three Neptune-mass planets system around HD 69830. *Astron. Astrophys.* 455, L25–L28.
- Andoyer, H., Mar. 1923. Cours de Mécanique Céleste. Gauthier-Villars, Paris.
- Arras, P., Socrates, A., Jan. 2009. Thermal Tides in Short Period Exoplanets. ArXiv e-prints.
- Arras, P., Socrates, A., May 2010. Thermal Tides in Fluid Extrasolar Planets. *Astrophys. J.* 714, 1–12.
- Avduevskii, V. S., Golovin, I. M., Zavelevich, F. S., Likhushin, V. I., Marov, M. I., Melnikov, D. A., Merson, I. I., Moshkin, B. E., Razin, K. A., Chernoshchekov, L. I., Sep. 1976. Preliminary results of an investigation of the light regime in the atmosphere and on the surface of Venus. *Kosmicheskie Issledovaniia* 14, 735–742.
- Banfield, D., Murray, N., Oct. 1992. A dynamical history of the inner Neptunian satellites. *Icarus* 99, 390–401.
- Barnes, J. R., Barman, T. S., Jones, H. R. A., Barber, R. J., Hansen, B. M. S., Prato, L., Rice, E. L., Leigh, C. J., Cameron, A. C., Pinfield, D. J., Jan. 2010. A search for molecules in the atmosphere of HD 189733b. *Mon. Not. R. Astron. Soc.* 401, 445–454.
- Bonfils, X., Mayor, M., Delfosse, X., Forveille, T., Gillon, M., Perrier, C., Udry, S., Bouchy, F., Lovis, C., Pepe, F., Queloz, D., Santos, N. C., Bertaux, J.-L., Oct. 2007. The HARPS search for southern extra-solar planets. X. A $m \sin i = 11 M_{\oplus}$ planet around the nearby spotted M dwarf GJ 674. *Astron. Astrophys.* 474, 293–299.
- Bouchy, F., Mayor, M., Lovis, C., Udry, S., Benz, W., Bertaux, J., Delfosse, X., Mordasini, C., Pepe, F., Queloz, D., Segransan, D., Mar. 2009. The HARPS

- search for southern extra-solar planets. XVII. Super-Earth and Neptune-mass planets in multiple planet systems HD 47 186 and HD 181 433. *Astron. Astrophys.* 496, 527–531.
- Boué, G., Laskar, J., Dec. 2006. Precession of a planet with a satellite. *Icarus* 185, 312–330.
- Boué, G., Laskar, J., Mar. 2010. A Collisionless Scenario for Uranus Tilting. *Astrophys. J.* 712, L44–L47.
- Boué, G., Laskar, J., Kuchynka, P., Sep. 2009. Speed Limit on Neptune Migration Imposed by Saturn Tilting. *Astrophys. J.* 702, L19–L22.
- Brouwer, D., Clemence, G. M., 1961. *Methods of celestial mechanics*. Academic Press, New York.
- Campbell, J. K., Anderson, J. D., May 1989. Gravity field of the Saturnian system from Pioneer and Voyager tracking data. *Astron. J.* 97, 1485–1495.
- Canup, R. M., Jan. 2005. A Giant Impact Origin of Pluto-Charon. *Science* 307, 546–550.
- Canup, R. M., Asphaug, E., Aug. 2001. Origin of the Moon in a giant impact near the end of the Earth’s formation. *Nature* 412, 708–712.
- Carpenter, R. L., Feb. 1964. Symposium on Radar and Radiometric Observations of Venus during the 1962 Conjunction: Study of Venus by CW radar. *Astron. J.* 69, 2–11.
- Carpenter, R. L., Feb. 1970. A Radar Determination of the Rotation of Venus. *Astron. J.* 75, 61–66.
- Cester, B., Ferluga, S., Boehm, C., Oct. 1983. The empirical mass-luminosity relation. *Astrophys. Space Sci.* 96, 125–140.
- Chapman, S., Lindzen, R., 1970. *Atmospheric tides. Thermal and gravitational*. Dordrecht: Reidel, 1970.
- Chirikov, B. V., 1979. A universal instability of many dimensional oscillator systems. *Physics Reports* 52, 263–379.
- Colombo, G., 1965. Rotational Period of the Planet Mercury. *Nature* 208, 575–578.
- Colombo, G., Shapiro, I. I., Jul. 1966. The Rotation of the Planet Mercury. *Astrophys. J.* 145, 296–307.
- Correia, A. C. M., Dec. 2006. The core-mantle friction effect on the secular spin evolution of terrestrial planets. *Earth Planet. Sci. Lett.* 252, 398–412.
- Correia, A. C. M., Oct. 2009. Secular Evolution of a Satellite by Tidal Effect: Application to Triton. *Astrophys. J.* 704, L1–L4.
- Correia, A. C. M., Couetdic, J., Laskar, J., Bonfils, X., Mayor, M., Bertaux, J., Bouchy, F., Delfosse, X., Forveille, T., Lovis, C., Pepe, F., Perrier, C., Queloz, D., Udry, S., Feb. 2010. The HARPS search for southern extra-solar planets. XIX. Characterization and dynamics of the GJ 876 planetary system. *Astron. Astrophys.* 511, A21.
- Correia, A. C. M., Laskar, J., Jun. 2001. The four final rotation states of Venus. *Nature* 411, 767–770.
- Correia, A. C. M., Laskar, J., Nov. 2003a. Different tidal torques on a planet with a dense atmosphere and consequences to the spin dynamics. *J. Geophys. Res. (Planets)* 108 (E11), 5123–10.
- Correia, A. C. M., Laskar, J., May 2003b. Long-term evolution of the spin of Venus II. Numerical simulations. *Icarus* 163, 24–45.
- Correia, A. C. M., Laskar, J., Jun. 2004. Mercury’s capture into the 3/2 spin-orbit resonance as a result of its chaotic dynamics. *Nature* 429, 848–850.
- Correia, A. C. M., Laskar, J., 2006. Evolution of the spin of Mercury and its capture into the 3/2 spin-orbit resonance. In: 2005: Past Meets Present in Astronomy and Astrophysics. Proceedings of the 15th Portuguese National Meeting. ISBN: 981-256-887-5. Published by World Scientific Publishing Co., Pte. Ltd., Singapore, 2006. pp. 1–4.
- Correia, A. C. M., Laskar, J., May 2009. Mercury’s capture into the 3/2 spin-orbit resonance including the effect of core-mantle friction. *Icarus* 201, 1–11.
- Correia, A. C. M., Laskar, J., Feb. 2010. Long-term evolution of the spin of Mercury. I. Effect of the obliquity and core-mantle friction. *Icarus* 205, 338–355.
- Correia, A. C. M., Laskar, J., Néron de Surgy, O., May 2003. Long-term evolution of the spin of Venus I. Theory. *Icarus* 163, 1–23.
- Correia, A. C. M., Levrard, B., Laskar, J., Sep. 2008. On the equilibrium rotation of Earth-like extra-solar planets. *Astron. Astrophys.* 488, L63–L66.
- Counselman, C. C., Shapiro, I. I., 1970. Spin-Orbit resonance of Mercury. *Symposia Mathematica* 3, 121–169.
- Darwin, G. H., 1880. On the secular change in the elements of a satellite revolving around a tidally distorted planet. *Philos. Trans. R. Soc. London* 171, 713–891.
- Darwin, G. H., 1908. *Scientific Papers*. Cambridge University Press.
- Dermott, S. F., Malhotra, R., Murray, C. D., Nov. 1988. Dynamics of the Uranian and Saturnian satellite systems - A chaotic route to melting Miranda? *Icarus* 76, 295–334.

- Dickey, J. O., Bender, P. L., Faller, J. E., Newhall, X. X., Ricklefs, R. L., Ries, J. G., Shelus, P. J., Veillet, C., Whipple, A. L., Wiant, J. R., Williams, J. G., Yoder, C. F., Jul. 1994. Lunar Laser Ranging - a Continuing Legacy of the Apollo Program. *Science* 265, 482–490.
- Dobrovolskis, A. R., Jan. 1980. Atmospheric tides and the rotation of Venus. II - Spin evolution. *Icarus* 41, 18–35.
- Dobrovolskis, A. R., Ingersoll, A. P., Jan. 1980. Atmospheric tides and the rotation of Venus. I - Tidal theory and the balance of torques. *Icarus* 41, 1–17.
- Dones, L., Tremaine, S., May 1993. On the origin of planetary spins. *Icarus* 103, 67–92.
- Efroimsky, M., Williams, J. G., Jul. 2009. Tidal torques: a critical review of some techniques. *Celestial Mechanics and Dynamical Astronomy* 104, 257–289.
- Eggenberger, A., Udry, S., Mayor, M., Apr. 2004. Statistical properties of exoplanets. III. Planet properties and stellar multiplicity. *Astron. Astrophys.* 417, 353–360.
- Escribano, B., Vanyo, J., Tuval, I., Cartwright, J. H. E., González, D. L., Piro, O., Tél, T., Sep. 2008. Dynamics of tidal synchronization and orbit circularization of celestial bodies. *Phys. Rev. E* 78 (3), 036216.
- Fabrycky, D., Tremaine, S., Nov. 2007. Shrinking Binary and Planetary Orbits by Kozai Cycles with Tidal Friction. *Astrophys. J.* 669, 1298–1315.
- Ferraz-Mello, S., Rodríguez, A., Hussmann, H., May 2008. Tidal friction in close-in satellites and exoplanets: The Darwin theory re-visited. *Celestial Mechanics and Dynamical Astronomy* 101, 171–201.
- Fischer, D. A., Marcy, G. W., Butler, R. P., Vogt, S. S., Laughlin, G., Henry, G. W., Abouav, D., Peek, K. M. G., Wright, J. T., Johnson, J. A., McCarthy, C., Isaacson, H., Mar. 2008. Five Planets Orbiting 55 Cancri. *Astrophys. J.* 675, 790–801.
- Ford, E. B., Rasio, F. A., Feb. 2006. On the Relation between Hot Jupiters and the Roche Limit. *Astrophys. J.* 638, L45–L48.
- Ford, E. B., Seager, S., Turner, E. L., Aug. 2001. Characterization of extrasolar terrestrial planets from diurnal photometric variability. *Nature* 412, 885–887.
- Forveille, T., Bonfils, X., Delfosse, X., Gillon, M., Udry, S., Bouchy, F., Lovis, C., Mayor, M., Pepe, F., Perrier, C., Queloz, D., Santos, N., Bertaux, J.-L., Jan. 2009. The HARPS search for southern extra-solar planets. XIV. Gl 176b, a super-Earth rather than a Neptune, and at a different period. *Astron. Astrophys.* 493, 645–650.
- Gold, T., Soter, S., Nov. 1969. Atmospheric Tides and the Resonant Rotation of Venus. *Icarus* 11, 356–366.
- Goldreich, P., Murray, N., Longaretti, P. Y., Banfield, D., Aug. 1989. Neptune’s story. *Science* 245, 500–504.
- Goldreich, P., Peale, S., Aug. 1966. Spin-orbit coupling in the solar system. *Astron. J.* 71, 425–438.
- Goldreich, P., Peale, S. J., 1968. The Dynamics of Planetary Rotations. *Annu. Rev. Astron. Astrophys.* 6, 287–320.
- Goldreich, P., Soter, S., 1966. Q in the Solar System. *Icarus* 5, 375–389.
- Goldstein, H., 1950. *Classical mechanics*. Addison-Wesley, Reading.
- Goldstein, R. M., Feb. 1964. Symposium on Radar and Radiometric Observations of Venus during the 1962 Conjunction: Venus characteristics by earth-based radar. *Astron. J.* 69, 12–19.
- Goodman, J., Jan. 2009. Concerning thermal tides on hot Jupiters. ArXiv e-prints.
- Hamilton, D. P., Ward, W. R., Nov. 2004. Tilting Saturn. II. Numerical Model. *Astron. J.* 128, 2510–2517.
- Hays, J. D., Imbrie, J., Shackleton, N. J., Dec. 1976. Variations in the Earth’s Orbit: Pacemaker of the Ice Ages. *Science* 194, 1121–1132.
- Henning, W. G., O’Connell, R. J., Sasselov, D. D., Dec. 2009. Tidally Heated Terrestrial Exoplanets: Viscoelastic Response Models. *Astrophys. J.* 707, 1000–1015.
- Henrard, J., 1993. The adiabatic invariant in classical dynamics. In: *Dynamics Reported*. Springer Verlag, New York, pp. 117–235.
- Henrard, J., Murigande, C., 1987. Colombo’s top. *Celestial Mechanics* 40, 345–366.
- Hinderer, J., Legros, H., Pedotti, G., 1987. Atmospheric pressure torque and axial rotation of Venus. *Advances in Space Research* 7, 311–314.
- Howard, A. W., Johnson, J. A., Marcy, G. W., Fischer, D. A., Wright, J. T., Henry, G. W., Giguere, M. J., Isaacson, H., Valenti, J. A., Anderson, J., Piskunov, N. E., May 2009. The NASA-UC Eta-Earth Program. I. A Super-Earth Orbiting HD 7924. *Astrophys. J.* 696, 75–83.
- Imbrie, J., Jun. 1982. Astronomical theory of the Pleistocene ice ages - A brief historical review. *Icarus* 50, 408–422.
- Jones, H. R. A., Butler, R. P., Tinney, C. G., Marcy, G. W., Carter, B. D., Penny, A. J., McCarthy, C., Bailey, J., Jun. 2006. High-eccentricity planets from the Anglo-Australian Planet Search. *Mon. Not. R. Astron. Soc.* 369, 249–256.

- Joshi, M. M., Haberle, R. M., Reynolds, R. T., Oct. 1997. Simulations of the Atmospheres of Synchronously Rotating Terrestrial Planets Orbiting M Dwarfs: Conditions for Atmospheric Collapse and the Implications for Habitability. *Icarus* 129, 450–465.
- Kaula, W. M., 1964. Tidal dissipation by solid friction and the resulting orbital evolution. *Rev. Geophys.* 2, 661–685.
- Kinoshita, H., Apr. 1977. Theory of the rotation of the rigid earth. *Celestial Mechanics* 15, 277–326.
- Kiseleva, L. G., Eggleton, P. P., Mikkola, S., Oct. 1998. Tidal friction in triple stars. *Mon. Not. R. Astron. Soc.* 300, 292–302.
- Knutson, H. A., Charbonneau, D., Noyes, R. W., Brown, T. M., Gilliland, R. L., Jan. 2007. Using Stellar Limb-Darkening to Refine the Properties of HD 209458b. *Astrophys. J.* 655, 564–575.
- Kokubo, E., Ida, S., Dec. 2007. Formation of Terrestrial Planets from Protoplanets. II. Statistics of Planetary Spin. *Astrophys. J.* 671, 2082–2090.
- Kozai, Y., Nov. 1962. Secular perturbations of asteroids with high inclination and eccentricity. *Astron. J.* 67, 591–598.
- Lambeck, K., 1980. *The Earth's Variable Rotation: Geophysical Causes and Consequences*. Cambridge University Press.
- Laskar, J., Mar. 1989. A numerical experiment on the chaotic behaviour of the solar system. *Nature* 338, 237–238.
- Laskar, J., Dec. 1990. The chaotic motion of the solar system - A numerical estimate of the size of the chaotic zones. *Icarus* 88, 266–291.
- Laskar, J., 1996. Large Scale Chaos and Marginal Stability in the Solar System. *Celestial Mechanics and Dynamical Astronomy* 64, 115–162.
- Laskar, J., Correia, A. C. M., Dec. 2004. The Rotation of Extra-solar Planets. In: *ASP Conf. Ser.* 321: *Extrasolar Planets: Today and Tomorrow*. pp. 401–409.
- Laskar, J., Correia, A. C. M., Gastineau, M., Joutel, F., Levrard, B., Robutel, P., Aug. 2004a. Long term evolution and chaotic diffusion of the insolation quantities of Mars. *Icarus* 170, 343–364.
- Laskar, J., Joutel, F., Robutel, P., Feb. 1993. Stabilization of the earth's obliquity by the moon. *Nature* 361, 615–617.
- Laskar, J., Levrard, B., Mustard, J. F., Sep. 2002. Orbital forcing of the martian polar layered deposits. *Nature* 419, 375–377.
- Laskar, J., Robutel, P., Feb. 1993. The chaotic obliquity of the planets. *Nature* 361, 608–612.
- Laskar, J., Robutel, P., Joutel, F., Gastineau, M., Correia, A. C. M., Levrard, B., Dec. 2004b. A long-term numerical solution for the insolation quantities of the Earth. *Astron. Astrophys.* 428, 261–285.
- Laughlin, G., Deming, D., Langton, J., Kasen, D., Vogt, S., Butler, P., Rivera, E., Meschiari, S., Jan. 2009. Rapid heating of the atmosphere of an extrasolar planet. *Nature* 457, 562–564.
- Levrard, B., Correia, A. C. M., Chabrier, G., Baraffe, I., Selsis, F., Laskar, J., Jan. 2007a. Tidal dissipation within hot Jupiters: a new appraisal. *Astron. Astrophys.* 462, L5–L8.
- Levrard, B., Forget, F., Montmessin, F., Laskar, J., Oct. 2004. Recent ice-rich deposits formed at high latitudes on Mars by sublimation of unstable equatorial ice during low obliquity. *Nature* 431, 1072–1075.
- Levrard, B., Forget, F., Montmessin, F., Laskar, J., Jun. 2007b. Recent formation and evolution of northern Martian polar layered deposits as inferred from a Global Climate Model. *Journal of Geophysical Research (Planets)* 112 (E11), 6012.
- Lidov, M. L., Oct. 1962. The evolution of orbits of artificial satellites of planets under the action of gravitational perturbations of external bodies. *Plan. Space Sci.* 9, 719–759.
- Lidov, M. L., Ziglin, S. L., Jun. 1976. Non-restricted double-averaged three body problem in Hill's case. *Celestial Mechanics* 13, 471–489.
- Lovis, C., Mayor, M., Pepe, F., Alibert, Y., Benz, W., Bouchy, F., Correia, A. C. M., Laskar, J., Mordasini, C., Queloz, D., Santos, N. C., Udry, S., Bertaux, J.-L., Sivan, J.-P., May 2006. An extrasolar planetary system with three Neptune-mass planets. *Nature* 441, 305–309.
- MacDonald, G. J. F., 1964. Tidal friction. *Revs. Geophys.* 2, 467–541.
- Mardling, R. A., Dec. 2007. Long-term tidal evolution of short-period planets with companions. *Mon. Not. R. Astron. Soc.* 382, 1768–1790.
- Mayor, M., Bonfils, X., Forveille, T., Delfosse, X., Udry, S., Bertaux, J., Beust, H., Bouchy, F., Lovis, C., Pepe, F., Perrier, C., Queloz, D., Santos, N. C., Nov. 2009a. The HARPS search for southern extra-solar planets. XVIII. An Earth-mass planet in the GJ 581 planetary system. *Astron. Astrophys.* 507, 487–494.
- Mayor, M., Udry, S., Lovis, C., Pepe, F., Queloz, D., Benz, W., Bertaux, J.-L., Bouchy, F., Mordasini, C., Segransan, D., Jan. 2009b. The HARPS search for southern extra-solar planets. XIII. A planetary system with 3

- super-Earths (4.2, 6.9, and 9.2 M_J). *Astron. Astrophys.* 493, 639–644.
- Migaszewski, C., Goździewski, K., Jan. 2009. Secular dynamics of a coplanar, non-resonant planetary system under the general relativity and quadrupole moment perturbations. *Mon. Not. R. Astron. Soc.* 392, 2–18.
- Mignard, F., May 1979. The evolution of the lunar orbit revisited. I. *Moon and Planets* 20, 301–315.
- Mignard, F., Oct. 1980. The evolution of the lunar orbit revisited. II. *Moon and Planets* 23, 185–201.
- Mignard, F., Feb. 1981. Evolution of the Martian satellites. *Mon. Not. R. Astron. Soc.* 194, 365–379.
- Munk, W. H., MacDonald, G. J. F., 1960. *The Rotation of the Earth; A Geophysical Discussion*. Cambridge University Press.
- Murray, C. D., Dermott, S. F., 1999. *Solar System Dynamics*. Cambridge University Press.
- Naef, D., Latham, D. W., Mayor, M., Mazeh, T., Beuzit, J. L., Drukier, G. A., Perrier-Bellet, C., Queloz, D., Sivan, J. P., Torres, G., Udry, S., Zucker, S., Aug. 2001. HD 80606 b, a planet on an extremely elongated orbit. *Astron. Astrophys.* 375, L27–L30.
- Néron de Surgy, O., Laskar, J., Feb. 1997. On the long term evolution of the spin of the Earth. *Astron. Astrophys.* 318, 975–989.
- Pepe, F., Correia, A. C. M., Mayor, M., Tamuz, O., Couétdic, J., Benz, W., Bertaux, J.-L., Bouchy, F., Laskar, J., Lovis, C., Naef, D., Queloz, D., Santos, N. C., Sivan, J.-P., Sosnowska, D., Udry, S., Feb. 2007. The HARPS search for southern extra-solar planets. VIII. μ Arae, a system with four planets. *Astron. Astrophys.* 462, 769–776.
- Pettengill, G. H., Dyce, R. B., 1965. A Radar Determination of the Rotation of the Planet Mercury. *Nature* 206, 1240–1241.
- Rafikov, R. R., Sep. 2006. Atmospheres of Protoplanetary Cores: Critical Mass for Nucleated Instability. *Astrophys. J.* 648, 666–682.
- Ragozzine, D., Wolf, A. S., Jun. 2009. Probing the Interiors of very Hot Jupiters Using Transit Light Curves. *Astrophys. J.* 698, 1778–1794.
- Rivera, E. J., Lissauer, J. J., Butler, R. P., Marcy, G. W., Vogt, S. S., Fischer, D. A., Brown, T. M., Laughlin, G., Henry, G. W., Nov. 2005. A $\sim 7.5 M_{\oplus}$ Planet Orbiting the Nearby Star, GJ 876. *Astrophys. J.* 634, 625–640.
- Santos, N. C., Benz, W., Mayor, M., Oct. 2005. Extrasolar Planets: Constraints for Planet Formation Models. *Science* 310, 251–255.
- Schiaparelli, G. V., Dec. 1889. Sulla rotazione di Mercurio. *Astronomische Nachrichten* 123, 241–250.
- Schlichting, H. E., Sari, R., Mar. 2007. The Effect of Semi-collisional Accretion on Planetary Spins. *Astrophys. J.* 658, 593–597.
- Seager, S., Hui, L., Aug. 2002. Constraining the Rotation Rate of Transiting Extrasolar Planets by Oblateness Measurements. *Astrophys. J.* 574, 1004–1010.
- Selsis, F., Kasting, J., Levrard, B., Paillet, J., Ribas, I., Delfosse, X., Dec. 2007. Habitable planets around the star Gliese 581? *Astron. Astrophys.* 476, 1373–1387.
- Siebert, M., 1961. Atmospheric Tides. *Advances in Geophysics* 7, 105–187.
- Smart, W. M., 1953. *Celestial Mechanics*. London, New York, Longmans, Green.
- Smith, W. B., Feb. 1963. Radar observations of Venus, 1961 and 1959. *Astron. J.* 68, 15–21.
- Sotin, C., Grasset, A., Mocquet, A., Nov. 2007. Mass-radius curve for extrasolar Earth-like planets and ocean planets. *Icarus* 191, 337–351.
- Spiegel, D. S., Haiman, Z., Gaudi, B. S., Nov. 2007. On Constraining a Transiting Exoplanet’s Rotation Rate with Its Transit Spectrum. *Astrophys. J.* 669, 1324–1335.
- Takata, T., Stevenson, D. J., Oct. 1996. Despin Mechanism for Protoplanet Planets and Ionization State of Protoplanet Planetary Disks. *Icarus* 123, 404–421.
- Tamuz, O., Ségransan, D., Udry, S., Mayor, M., Eggenberger, A., Naef, D., Pepe, F., Queloz, D., Santos, N. C., Demory, B., Figuera, P., Marmier, M., Montagnier, G., Mar. 2008. The CORALIE survey for southern extra-solar planets. XV. Discovery of two eccentric planets orbiting HD 4113 and HD 156846. *Astron. Astrophys.* 480, L33–L36.
- Tisserand, F., 1891. *Traité de Mécanique Céleste (Tome II)*. Gauthier-Villars, Paris.
- Tittemore, W. C., Wisdom, J., Jun. 1990. Tidal evolution of the Uranian satellites. III - Evolution through the Miranda-Umbriel 3:1, Miranda-Ariel 5:3, and Ariel-Umbriel 2:1 mean-motion commensurabilities. *Icarus* 85, 394–443.
- Tokovinin, A., Thomas, S., Sterzik, M., Udry, S., May 2006. Tertiary companions to close spectroscopic binaries. *Astron. Astrophys.* 450, 681–693.
- Touma, J., Wisdom, J., Feb. 1993. The chaotic obliquity of Mars. *Science* 259, 1294–1297.

- Udry, S., Bonfils, X., Delfosse, X., Forveille, T., Mayor, M., Perrier, C., Bouchy, F., Lovis, C., Pepe, F., Queloz, D., Bertaux, J.-L., Jul. 2007. The HARPS search for southern extra-solar planets. XI. Super-Earths (5 and 8 M_{\oplus}) in a 3-planet system. *Astron. Astrophys.* 469, L43–L47.
- Veeder, G. J., Matson, D. L., Johnson, T. V., Blaney, D. L., Goguen, J. D., Aug. 1994. Io's heat flow from infrared radiometry: 1983-1993. *J. Geophys. Res.* 99, 17095–17162.
- Ward, W. R., Jan. 1975. Tidal friction and generalized Cassini's laws in the solar system. *Astron. J.* 80, 64–70.
- Ward, W. R., Hamilton, D. P., Nov. 2004. Tilting Saturn. I. Analytic Model. *Astron. J.* 128, 2501–2509.
- Williams, G. E., Apr. 1990. Precambrian Cyclic Rhythmites: Solar-Climatic or Tidal Signatures? *R. Soc. London Phil. Trans. A* 330, 445–457.
- Winn, J. N., Holman, M. J., Aug. 2005. Obliquity Tides on Hot Jupiters. *Astrophys. J.* 628, L159–L162.
- Wisdom, J., Jul. 2004. Spin-Orbit Secondary Resonance Dynamics of Enceladus. *Astron. J.* 128, 484–491.
- Wisdom, J., Peale, S. J., Mignard, F., May 1984. The chaotic rotation of Hyperion. *Icarus* 58, 137–152.
- Wu, Y., Murray, N., May 2003. Planet Migration and Binary Companions: The Case of HD 80606b. *Astrophys. J.* 589, 605–614.
- Yoder, C. F., Oct. 1995. Venus' free obliquity. *Icarus* 117, 250–286.
- Yoder, C. F., 1997. Venusian Spin Dynamics. In: *Venus II: Geology, Geophysics, Atmosphere, and Solar Wind Environment*. pp. 1087–1124.
- Zahn, J., Jul. 1975. The dynamical tide in close binaries. *Astron. Astrophys.* 41, 329–344.